

Encoding, decoding, and causality between complex networks*

Yang Tian,[†] Hedong Hou,[‡] Guangzheng Xu,[§] Ziyang Zhang,[¶] and Pei Sun^{**}

Complex networks are common in physics, biology, computer science, and social science. Quantifying the relations (e.g., similarity or difference) between complex networks paves the way for understanding the latent information shared across networks. However, fundamental metrics of relations, such as information divergence, mutual information, Fisher information, and causality, are not well-defined between complex networks. As a compromise, commonly used strategies (e.g., network embedding, matching, and kernel approaches) measure network relations in data-driven ways. These approaches are computation-oriented and inapplicable to analytic derivations in mathematics and physics. To resolve these issues, we present a theory to derive an optimal characterization of network topological properties. Our theory shows that a network can be fully represented by a Gaussian variable defined by a function of the discrete Schrödinger operator (i.e., the Laplacian), which simultaneously satisfies network-topology-dependent smoothness and maximum entropy properties. Based on this characterization, we can analytically measure diverse relations between complex networks in terms of topology properties. As illustrations, we primarily show how to define encoding (e.g., information divergence and mutual information), decoding (e.g., Fisher information), and causality (e.g., transfer entropy and Granger causality) between complex networks. We validate our framework on representative complex networks (e.g., evolutionary random network models, protein-protein interaction network, and chemical compound networks), and demonstrate that a series of science and engineering challenges (e.g., network evolution, clustering, and classification) can be tackled from a new perspective. A computationally efficient implementation of our theory is released as an open-source multi-platform toolbox.

I. INTRODUCTION

Complex networks exist universally across different disciplines [1]. Important topics in physics (e.g., quantum system characterization [2–4] and non-equilibrium dynamics analysis [5–7]), biology (e.g., brain [8–12], metabolic [13–15], and protein [16–18] networks analysis), computer science (e.g., internet analysis [19–21] and information tracking [22, 23]), and social science (e.g., scientific community analysis [24–26] and opinion formation modelling [27–29]) would benefit from studying complex networks [1] and, therefore, promote the rapid development of network theories.

However, critical challenges to network theories persistently arise due to the increasingly diverse application needs [1]. Among these challenges, a fundamental yet intractable one concerns how to quantify the relations (e.g.,

similarity) between different complex networks [30]. To date, mainstream metrics of network relations are developed in the contexts of network embedding, matching, and kernel, three computation-oriented and data-driven perspectives [30, 31]. Comprehensive reviews of these three perspectives can be found in Refs. [30, 32], Refs. [33–35], and Refs. [36, 37], respectively. In general, *embedding-based* approaches embed networks into low-dimensional metric spaces (e.g., future vectors) following preset rules to calculate distances between networks or classify networks [30–32]. Therefore, these approaches critically depend on embedding rule designs and may lack universal principles to guarantee their generalization capacities [30]. *Matching-based* approaches, such as exact [38] and inexact [36] matching with and without edge-preserving properties, search for node mappings between networks to realize optimal matching and measure similarity [34]. These approaches essentially deal with a kind of quadratic programming problems [33, 39, 40] that are NP-hard [33] and require relaxations of problem constraints to find approximate solutions (e.g., see Refs. [41–43] for approximation). *Kernel-based* methods evaluate the similarity between networks by decomposing them into series of atomic substructures (e.g., graphlets [44], random walks [45], shortest paths [46], and cycles [47]) and measuring kernel value among these substructures (i.e., counting the number of shared substructures) [36, 37]. While these substructures generally reflect network topology properties, they are essentially handcrafted [31], i.e., extracted by certain manually defined functions, and may imply extremely high-dimensional, sparse, and non-smooth representations of large-scale networks with poor generalization capacities [48]. In sum, while embedding-, matching-, and kernel-

* Correspondence should be addressed to P.S.

[†] tiany20@mails.tsinghua.edu.cn; Department of Psychology & Tsinghua Laboratory of Brain and Intelligence, Tsinghua University, Beijing, 100084, China.; Also at Laboratory of Advanced Computing and Storage, Central Research Institute, 2012 Laboratories, Huawei Technologies Co. Ltd., Beijing, 100084, China.

[‡] hedong.hou@etu.u-paris.fr; Institut de Mathématiques d'Orsay, Institut de Mathématiques d'Orsay, 14 Rue Joliot-Curie, 91190 Gif-sur-Yvette, France.

[§] gzxu98@gmail.com; Department of Computer Science, University College London, London, WC1E 6AE, UK.

[¶] zhangziyang11@huawei.com; Laboratory of Advanced Computing and Storage, Central Research Institute, 2012 Laboratories, Huawei Technologies Co. Ltd., Beijing, 100084, China.

^{**} peisun@tsinghua.edu.cn; Department of Psychology & Tsinghua Brain and Intelligence Lab, Tsinghua University, Beijing, 100084, China.

based approaches have been extensively tested on empirical data (e.g., on neural data [37, 49–51]), they are inevitably limited by computational complexity (e.g., matching-based) or the dependence on empirical choice of network features (e.g., embedding-based) and kernel functions (e.g., kernel-based) [49]. Even in cases where these methods are computationally optimal, they may still be unsatisfactory because they do not derive intrinsic relations between complex networks analytically and universally.

Analytic metrics of network relations are indispensable for developing mathematics and statistic physics of complex networks [52] but remain largely unknown yet. Certainly, one can simplify the distance between networks as the Kolmogorov–Smirnov statistic between their degree distributions (e.g., see discussions in [50]). However, two networks with the same degree distribution can still have distinct topology properties because edge wring rules are not completely determined by the degree distribution.

To suggest a possible way to define analytic and universal network relations, here we develop a theory of an optimal characterization of complex networks that simultaneously ensures smoothness (for optimal reflection of network topology [53–56]) and maximum entropy (for better support of information-theoretical analysis [57]) properties in Secs. II–III. The derived characterizations turn out to be specific Gaussian variables defined by the functions of discrete Schrödinger operators of complex networks. Based on this result, we can define analytic relation metrics (e.g., information divergence [57], mutual information [57], Fisher information [57], and causality [58]) between complex networks in Sec. IV and explore their potential generalization in Sec. V. In Secs. VI–VII, we demonstrate our approach on representative networks (e.g., random network models, a protein-protein interaction network, and chemical compound networks) to define encoding, decoding, and causal analyses between them, which raise potential insights on related science and engineering questions. In Sec. VIII, we discuss the advantages and deficiencies of our theory and suggest future directions for improvements. An open-source toolbox of our work is provided in Ref. [59].

II. QUESTION DEFINITION

An appropriate question definition is more important than the answer itself. To suggest a potential direction, we consider following questions:

- (I) How to develop an analytic and universal characterization of network topology that is free of subjective selection of topological properties and computational optimization problems?
- (II) How to enable the characterization derived in question (I) to define analytic metrics of network relation (e.g., information divergence [57], mutual in-

formation [57], Fisher information [57], and causality [58]) without further constraints?

Clearly, question (II) requires a probabilistic solution (e.g., define a network as a random variable) of question (I). This idea inspires us to consider a mapping $\phi : V \rightarrow \Omega$ between a network $\mathcal{G}(V, E)$ without self-loops and a probability space $(\Omega, \mathcal{F}, \mathcal{P})$ with $\Omega = \mathbb{R}$. Here V and E denote the node and edge sets of network \mathcal{G} , respectively. Function ϕ defines a random variable $\mathcal{X}_\phi = (X_\phi(1), \dots, X_\phi(n))$ distributed on node set V , where $X_\phi(i) = \phi(v_i)$ and $n = |V|$ (see **Fig. 1** for illustrations).

To properly reflect the network topology of \mathcal{G} by \mathcal{X}_ϕ , we need to consider the *smoothness* of mapping ϕ on \mathcal{G} measured by the *discrete 2-Dirichlet form* of ϕ [54]

$$\mathcal{S}(\phi) = \frac{1}{2} \sum_{v_i \in V} \sum_{(v_i, v_j) \in E} \left(\frac{\partial \phi}{\partial (v_i, v_j)} \Big|_{v_i} \right)^2, \quad (1)$$

where (v_i, v_j) denotes the edge between nodes v_i and v_j . In Eq. (1), the edge derivative of ϕ with respect to edge (v_i, v_j) at node v_i is defined as [54]

$$\frac{\partial \phi}{\partial (v_i, v_j)} \Big|_{v_i} = \sqrt{W_{i,j}} (X_\phi(j) - X_\phi(i)), \quad (2)$$

where W is the non-negative weighted adjacent matrix of \mathcal{G} . The smaller $\mathcal{S}(\phi)$ in Eq. (1) is, the smoother ϕ is on \mathcal{G} . To understand why the smoothness of ϕ matters in defining \mathcal{X}_ϕ to reflect the network topology of \mathcal{G} , we need to consider the combinatorial graph Laplacian L , a kind of *discrete Schrödinger operator* [60], of \mathcal{G}

$$L = \text{diag}([\deg(v_1), \dots, \deg(v_n)]) - W, \quad (3)$$

where $\text{diag}(\cdot)$ generates a diagonal matrix and operator $\deg(\cdot)$ measures node degree. Note that $\deg(v_i) = \sum_{j=1}^n W_{ij}$ in a weighted network. Laplacian L captures key topology information of network \mathcal{G} (e.g., connected components, random walks on network, and latent Laplace–Beltrami operator [61]), which has been extensively used in spectral graph theory [61] and graph signal theory [54]. The first connection between Laplacian L and the smoothness of ϕ is well-known [54]

$$\mathcal{S}(\phi) = \mathcal{X}_\phi^T L \mathcal{X}_\phi, \quad (4)$$

which suggests that the smoothness of ϕ can be defined by Laplacian L (see **Fig. 1**). The second connection is derived from the Courant–Fischer theorem [62]. Letting $\{\psi_1, \dots, \psi_n\}$ and $\{\lambda_1, \dots, \lambda_n\}$ be the eigenvectors and eigenvalues of Laplacian L , one can use the Rayleigh quotient to derive that $\lambda_1 = \min\{\mathcal{X}_\phi^T L \mathcal{X}_\phi \mid \mathcal{X}_\phi \in \mathbb{R}^n, \|\mathcal{X}_\phi\|_2 = 1\}$ and $\lambda_i = \min\{\mathcal{X}_\phi^T L \mathcal{X}_\phi \mid \mathcal{X}_\phi \in \mathbb{R}^n, \|\mathcal{X}_\phi\|_2 = 1, \mathcal{X}_\phi \perp \text{span}(\psi_1, \dots, \psi_{i-1})\}$ (here $2 \leq i \leq n$) [54]. This property demonstrates that the smoothness of ϕ is related to the eigenvectors and eigenvalues of Laplacian L . Eigenvectors with smaller eigenvalues imply a smoother mapping ϕ . Taken together,

the smoothness of ϕ matters in our analysis because it is closely related to the topology information conveyed by Laplacian L . To enable variable \mathcal{X}_ϕ to represent network \mathcal{G} , we expect that the smoothness of ϕ is completely determined by the topology properties of \mathcal{G} .

To properly measure information quantities (e.g., mutual information) between complex networks applying \mathcal{X}_ϕ , the upper bounds of these quantities in \mathcal{X}_ϕ should not be too small. Otherwise, these quantities may be easily covered by noises in empirical data due to their small orders of magnitude. To precisely understand why large upper bounds are necessary, we consider the mutual information $\mathcal{I}(\mathcal{X}_\phi^i; \mathcal{X}_\phi^j)$ between two networks \mathcal{G}_i and \mathcal{G}_j as an instance. It is trivial that $\mathcal{I}(\mathcal{X}_\phi^i; \mathcal{X}_\phi^j) \leq \min\{\mathcal{H}(\mathcal{X}_\phi^i), \mathcal{H}(\mathcal{X}_\phi^j)\}$, where $\mathcal{H}(\cdot)$ denotes the Shannon entropy [57]. Therefore, $\mathcal{I}(\mathcal{X}_\phi^i; \mathcal{X}_\phi^j)$ may be frequently clouded by noises or directly vanish given small quantities of $\mathcal{H}(\mathcal{X}_\phi^i)$ and $\mathcal{H}(\mathcal{X}_\phi^j)$. In the present study, we primarily focus on the Shannon entropy because extensive information upper bounds are related to it [57]. This idea inspires us to consider maximum entropy distribution problem [57] while defining mapping ϕ (see **Fig. 1**).

In summary, an appropriate solution of questions (I-II) requires us to consider the smoothness and maximum entropy properties of mapping ϕ . Below, we suggest a potential solution.

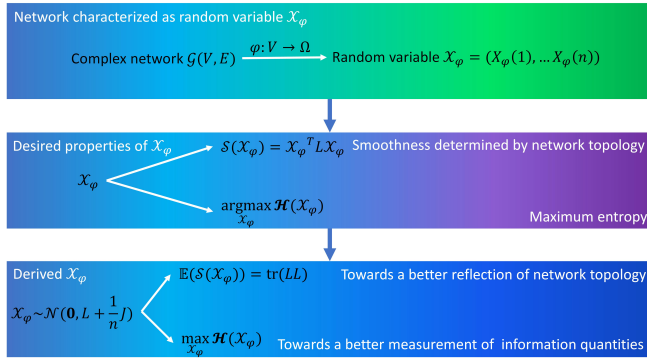


FIG. 1. General ideas of solving questions (I-II). We begin with defining a random variable \mathcal{X}_ϕ on network \mathcal{G} based on mapping ϕ . An ideal definition of \mathcal{X}_ϕ is expected to make the smoothness of mapping ϕ be completely determined by network topology. Meanwhile, it is expected to ensure the maximum entropy property of variable \mathcal{X}_ϕ . According to our derivations, we suggest $\mathcal{X}_\phi \sim \mathcal{N}(\mathbf{0}, L + \frac{1}{n} J)$ as a possible solution.

III. GAUSSIAN VARIABLE DEFINED BY THE FUNCTION OF DISCRETE SCHRÖDINGER OPERATOR

To avoid that $\mathcal{S}(\phi)$ in Eq. (1) diverges, random variable \mathcal{X}_ϕ is expected to have finite 1-st and 2-nd moments on each dimension. In our theory, we suggest a possible scheme

$$\mathbb{E}(\mathcal{X}_\phi) = \mathbf{0}, \quad (5)$$

$$\mathbb{D}(\mathcal{X}_\phi) = \Sigma \in \mathbb{R}^{n \times n}, \quad (6)$$

where $\mathbf{0} = (0, \dots, 0)$ is a vector of zeros, $\mathbb{E}(\cdot)$ denotes the 1-st moment, and $\mathbb{D}(\cdot)$ denotes the 2-nd moment. Given Eqs. (5-6), we can reformulate Eq. (1) as

$$\mathbb{E}(\mathcal{S}(\phi)) = \sum_{(v_i, v_j) \in E} \sqrt{W_{i,j}} (\Sigma_{ii} + \Sigma_{jj} - 2\Sigma_{ij}), \quad (7)$$

where W , the weighted adjacent matrix, is predetermined by a given network. In Eq. (7), matrix Σ is the only one adjustable term. To ensure the effectiveness of \mathcal{X}_ϕ in reflecting the topology information of \mathcal{G} , we suggest to choose matrix Σ as

$$\Sigma = L + \frac{1}{n} J, \quad (8)$$

where J is an all-one matrix. The motivation of the above definition lies in four aspects. First, although L is a singular matrix, previous studies have proven that $L + \frac{1}{n} J$ is invertible [63, 64]

$$\left(L + \frac{1}{n} J \right)^{-1} = L^\dagger + \frac{1}{n} J, \quad (9)$$

where \dagger denotes the Moore–Penrose pseudoinverse that satisfy $LL^\dagger L = L$ [65]. This property ensures the possibility to calculate numerous quantities defined with Σ^{-1} in Sec. IV. Second, Eqs. (8-9) relate Σ with L^\dagger directly. The pseudoinverse Laplacian L^\dagger is the *reproducing kernel* of $\mathbb{H}(\mathcal{G})$, the Hilbert space of real-valued functions over the node set $f_{\mathcal{G}}: V \rightarrow \mathbb{R}^n$ whose inner product is $\langle f_{\mathcal{G}}, g_{\mathcal{G}} \rangle = f_{\mathcal{G}}^T L g_{\mathcal{G}}$ [66, 67]. Because L^\dagger is unique for $\mathbb{H}(\mathcal{G})$, we can confirm a unique $\mathbb{H}(\mathcal{G})$ given L^\dagger . This property lays foundations for kernel tricks [68–70] on network \mathcal{G} when future studies explore machine learning tasks on random variable \mathcal{X}_ϕ (e.g., see kernel tricks in causality analysis [71, 72]). Third, Laplacian L and its pseudoinverse L^\dagger directly determine various topology properties of \mathcal{G} (e.g., network coherence [73], node importance [74], and the number of spanning trees [61]). Therefore, Eqs. (8-9) ensure the expressive ability of \mathcal{X}_ϕ about network topology. Fourth, we can apply Eq. (4) to derive the quadratic form

$$\mathbb{E}(\mathcal{S}(\phi)) = \mathbb{E}(\mathcal{X}_\phi)^T L \mathbb{E}(\mathcal{X}_\phi) + \text{tr}(L\Sigma), \quad (10)$$

$$= \text{tr} \left[L \left(L + \frac{1}{n} J \right) \right], \quad (11)$$

if Eq. (8) holds. If network \mathcal{G} is connected (i.e., there is only one zero eigenvalue in $\{\lambda_1, \dots, \lambda_n\}$), we can further apply $LL^\dagger = L^\dagger L = I - \frac{1}{n}J$ [64, 74, 75], where I is the unit matrix, to derive

$$\mathbb{E}(\mathcal{S}(\phi)) = \text{tr} [LL + L(I - L^\dagger L)], \quad (12)$$

$$= \text{tr}(LL + L - LL^\dagger L), \quad (13)$$

$$= \text{tr}(LL). \quad (14)$$

Eq. (11) and Eq. (14) suggest a benefit of Eq. (8) that we can control the expected smoothness of ϕ on a network completely by Laplacian L (see **Fig. 1**).

To ensure the maximum entropy property, we need to analyze the maximum entropy distribution problem. Considering a random variable $\mathcal{X}_\phi \in \mathbb{R}^n$ with finite 1-st and 2-nd moments defined in Eqs. (5-6), we can know that

$$\mathcal{H}(\mathcal{X}_\phi) \leq \mathcal{H}(\mathcal{N}(\mathbf{0}, \Sigma)), \quad (15)$$

where $\mathcal{N}(\mathbf{0}, \Sigma)$ is the n -dimensional Gaussian distribution. Eq. (15) is derived from the fact that the maximum entropy distribution defined on \mathbb{R}^n with given 1-st and 2-nd moments in Eqs. (5-6) is the Gaussian distribution [57]. Therefore, we define random variable \mathcal{X}_ϕ as

$$\mathcal{X}_\phi \sim \mathcal{N}\left(\mathbf{0}, L + \frac{1}{n}J\right) \quad (16)$$

to reflect the topology information of network \mathcal{G} (see **Fig. 1**). In practice, we can readily derive the accurate entropy value

$$\mathcal{H}(\mathcal{X}_\phi) = \frac{n}{2} + \frac{n}{2} \ln(2\pi) + \frac{1}{2} \ln \left[\det \left(L + \frac{1}{n}J \right) \right], \quad (17)$$

where $\det(\cdot)$ denotes the determinant.

In sum, an appropriate solution of questions (I-II) requires us to represent network $\mathcal{G}(V, E)$ by a Gaussian variable in Eq. (13), which ensures the topology-dependent smoothness and maximum entropy properties of mapping ϕ (see **Fig. 1**). Such a variable is completely characterized by a function of the discrete Schrödinger operator of the network [60], whose precision matrix (the inverse of covariance matrix) is $L^\dagger + \frac{1}{n}J$.

Surprisingly, we notice that our result in Eq. (13) is similar with the graph signal characterization [76, 77] derived by factor analysis [78] and low-rank models [79, 80] in the field of engineering, which states that a Gaussian Markov random field representation (a special type of Gaussian variable) improves graph Laplacian learning in practice [76, 77]. The main difference between Refs. [76, 77] and our work lies in that they pre-set the covariance matrix as $\Sigma = L^\dagger$ while we define $\Sigma = L + \frac{1}{n}J$. This similarity suggests the validity of our ideas from the perspective of computation practice. In Sec. VIII C, we present a more comprehensive comparison between our results and previous studies [76, 77] from the perspective of graph signal.

IV. ANALYTIC METRICS OF NETWORK RELATIONS

After representing two complex networks \mathcal{G}_a and \mathcal{G}_b by Gaussian variables $\mathcal{X}_\phi^a = (X_\phi^a(1), \dots, X_\phi^a(n)) \sim \mathcal{N}(\mathbf{0}, L(a) + \frac{1}{n}J)$ and $\mathcal{X}_\phi^b = (X_\phi^b(1), \dots, X_\phi^b(n)) \sim \mathcal{N}(\mathbf{0}, L(b) + \frac{1}{n}J)$, we can develop analytic metrics of network relations, such as information divergence, mutual information, Fisher information, and causality (e.g., transfer entropy and Granger causality). Because the all-one matrix J frequently occurs in our derivations, we make a convention that J has the same size with matrix A whenever we calculate $A + J$. The notions of matrix sizes are omitted for convenience.

A. Encoding: information divergence and mutual information

For information divergence (or referred to as the Kullback–Leibler divergence [57]), we can formulate it in a conventional form

$$\mathcal{D}(\mathcal{X}_\phi^a \parallel \mathcal{X}_\phi^b) = \mathbb{E}_{\rho_a} [\log(\rho_a) - \log(\rho_b)], \quad (18)$$

where ρ_a and ρ_b are probability densities of \mathcal{X}_ϕ^a and \mathcal{X}_ϕ^b , respectively (see **Fig. 2**). Because \mathcal{X}_ϕ^a and \mathcal{X}_ϕ^b are Gaussian variables, we can derive

$$\begin{aligned} \log(\rho_a) &= -\frac{1}{2} \log \left[(2\pi)^n \det \left(L(a) + \frac{1}{n}J \right) \right] \\ &\quad - \frac{1}{2} [\mathcal{X}_\phi^a]^T \left(L^\dagger(a) + \frac{1}{n}J \right) \mathcal{X}_\phi^a, \end{aligned} \quad (19)$$

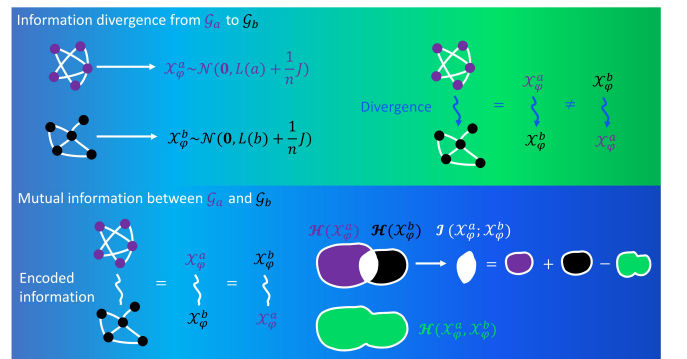


FIG. 2. Conceptual illustrations of information divergence and mutual information between complex networks. The information divergence from network \mathcal{G}_a to network \mathcal{G}_b , defined by $\mathcal{D}(\mathcal{X}_\phi^a \parallel \mathcal{X}_\phi^b)$ in Eq. (20), is not necessarily equal to the information divergence from network \mathcal{G}_b to network \mathcal{G}_a (upper parallel). The mutual information between networks \mathcal{G}_a and \mathcal{G}_b , defined by $\mathcal{I}(\mathcal{X}_\phi^a; \mathcal{X}_\phi^b)$ in Eq. (21), can be understood as the shared part of entropy quantities $\mathcal{H}(\mathcal{X}_\phi^a)$ and $\mathcal{H}(\mathcal{X}_\phi^b)$ (bottom parallel).

which readily leads to

$$\mathcal{D}(\mathcal{X}_\phi^a \parallel \mathcal{X}_\phi^b) = \frac{1}{2} \left[\text{tr} \left[\left(L^\dagger(b) + \frac{1}{n} J \right) \left(L(a) + \frac{1}{n} J \right) \right] - n + \ln \frac{\det(L(b) + \frac{1}{n} J)}{\det(L(a) + \frac{1}{n} J)} \right]. \quad (20)$$

Eq. (20) measures the directional difference between the topology of \mathcal{G}_a and \mathcal{G}_b . The difference is directional since $\mathcal{D}(\mathcal{X}_\phi^a \parallel \mathcal{X}_\phi^b) \neq \mathcal{D}(\mathcal{X}_\phi^b \parallel \mathcal{X}_\phi^a)$ (see Fig. 2).

For mutual information $\mathcal{I}(\mathcal{X}_\phi^a; \mathcal{X}_\phi^b)$ that quantifies the topology information of network \mathcal{G}_a encoded by network \mathcal{G}_b , we can calculate (see Fig. 2)

$$\mathcal{I}(\mathcal{X}_\phi^a; \mathcal{X}_\phi^b) = \mathcal{H}(\mathcal{X}_\phi^a) + \mathcal{H}(\mathcal{X}_\phi^b) - \mathcal{H}(\mathcal{X}_\phi^a, \mathcal{X}_\phi^b), \quad (21)$$

where $\mathcal{H}(\mathcal{X}_\phi^a)$ and $\mathcal{H}(\mathcal{X}_\phi^b)$ can be measured based on Eq. (17). A challenge in Eq. (21) lies in that $\mathcal{H}(\mathcal{X}_\phi^a, \mathcal{X}_\phi^b)$ is non-trivial for analytic derivations unless variables $X_\phi^a(i)$ and $X_\phi^b(j)$ are jointly Gaussian (this enables $\mathcal{H}(\mathcal{X}_\phi^a, \mathcal{X}_\phi^b)$ to be defined by Eq. (17) as well). In practice, we can generate samples of $\mathcal{X}_\phi^a \sim \mathcal{N}(\mathbf{0}, L(a) + \frac{1}{n} J)$ and $\mathcal{X}_\phi^b \sim \mathcal{N}(\mathbf{0}, L(b) + \frac{1}{n} J)$ by inverse transform sampling [81] to estimate $\mathcal{H}(\mathcal{X}_\phi^a, \mathcal{X}_\phi^b)$ using the Kozachenko-Leonenko estimator of Shannon entropy [82, 83].

B. Decoding: Fisher information

For Fisher information, we assume that a parameter vector $\Theta = (\theta_1, \dots, \theta_k) \in \mathbb{R}^k$ controlled by network

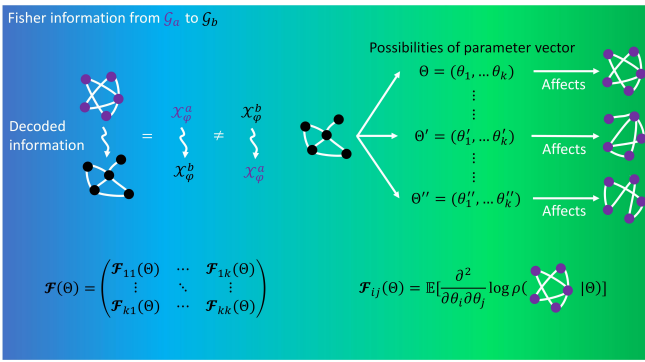


FIG. 3. Conceptual illustrations of Fisher information between complex networks. The (i, j) element in the Fisher information matrix, denoted by $\mathcal{F}_{ij}(\Theta)$ in Eq. (22), can be understood as the information that network \mathcal{G}_a carries about the parameter vector Θ controlled by network \mathcal{G}_b . The information is contained in $\rho_a(\cdot | \Theta)$, the probability distribution of variable \mathcal{X}_ϕ^a that is affected by Θ . The information quantity can be understood as the mean sensitivity of $\rho_a(\cdot | \Theta)$ towards the variation of Θ .

\mathcal{G}_b can affect the discrete Schrödinger operator $L(a)$ of network \mathcal{G}_a . Fisher information measures how precisely we can decode the topology information of \mathcal{G}_a from \mathcal{G}_b according to parameter vector Θ . We denote $\mathcal{X}_\phi^a \sim \mathcal{N}(\mathbf{0}, L^\dagger(a | \Theta))$ as the Gaussian variable given parameter vector Θ (see Fig. 3). Then we can have a special form of Fisher information matrix depending on the covariance matrix [84, 85]

$$\mathcal{F}_{ij}(\Theta) = - \int \rho_a(\chi; \Theta) \left\{ \frac{\partial^2}{\partial \theta_i \partial \theta_j} \log [\rho_a(\chi | \Theta')] \right\}_{\Theta'=\Theta} d\chi, \quad (22)$$

$$= \frac{1}{2} \text{tr} \left[\left(L^\dagger(a | \Theta) + \frac{1}{n} J \right) \frac{\partial L(a | \Theta)}{\partial \theta_i} \right. \\ \left. \times \left(L^\dagger(a | \Theta) + \frac{1}{n} J \right) \frac{\partial L(a | \Theta)}{\partial \theta_j} \right], \quad (23)$$

where $\rho_a(\cdot | \Theta)$ is the probability density of \mathcal{X}_ϕ^a given Θ (see Fig. 3). We define

$$\frac{\partial L(a; \Theta)}{\partial \theta_i} = \begin{bmatrix} \frac{\partial L_{11}(a | \Theta)}{\partial \theta_i} & \dots & \frac{\partial L_{1n}(a | \Theta)}{\partial \theta_i} \\ \vdots & \ddots & \vdots \\ \frac{\partial L_{n1}(a | \Theta)}{\partial \theta_i} & \dots & \frac{\partial L_{nn}(a | \Theta)}{\partial \theta_i} \end{bmatrix}. \quad (24)$$

The expectation vector does not occur in Eq. (23) because \mathcal{X}_ϕ^a always has zero expectation value on each dimension. In application, one can further calculate Fisher information quantity, $\text{tr}[\mathcal{F}(\Theta)]$, as a metric of decoding precision.

C. Causality: Granger causality and transfer entropy

To this point, we have analytically derived information divergence, mutual information, and Fisher information between complex networks. These metrics lay the foundation of encoding and decoding analyses on network ensembles. Compared with these analyses, causality is more difficult to study between networks because it is initially analyzed on time series [58]. Although dynamic networks feature time domain evolution [86–88], most networks lack a well-defined concept of time (e.g., networks may be static). To develop applicable causality metrics for arbitrary networks, we explore possible generalization of the mainstream causality metrics, such as transfer entropy [89–91] and Granger causality [92–95], from time domain to graph domain.

Let us begin with a classic form of Granger causality analyzed by regression models. Our basic idea is to consider a random partition on network \mathcal{G}_a to divide it into two sub-networks, \mathcal{G}_a^o and \mathcal{G}_a^* . This is equivalent to dividing random variable $\mathcal{X}_\phi^a = (X_\phi^a(1), \dots, X_\phi^a(n))$ into two

sub-vectors of multivariate Gaussian random variables $\mathcal{X}_\phi^{a,\circ}$ and $\mathcal{X}_\phi^{a,\star}$. Without loss of generality, we set $\mathcal{X}_\phi^{a,\circ} = (X_\phi^a(1), \dots, X_\phi^a(k)) \sim \mathcal{N}(\mathbf{0}, L(a, \circ) + \frac{1}{n}J)$ and $\mathcal{X}_\phi^{a,\star} = (X_\phi^a(k+1), \dots, X_\phi^a(n)) \sim \mathcal{N}(\mathbf{0}, L(a, \star) + \frac{1}{n}J)$, where we know

$$L(a, \circ) = \begin{bmatrix} L_{11}(a) & \dots & L_{1k}(a) \\ \vdots & \ddots & \vdots \\ L_{k1}(a) & \dots & L_{kk}(a) \end{bmatrix}, \quad (25)$$

$$L(a, \star) = \begin{bmatrix} L_{(k+1)(k+1)}(a) & \dots & L_{(k+1)n}(a) \\ \vdots & \ddots & \vdots \\ L_{n(k+1)}(a) & \dots & L_{nn}(a) \end{bmatrix}, \quad (26)$$

and we can represent $L(a)$ in a block matrix form $L(a) = \begin{bmatrix} L(a, \circ) & L(a, \triangle) \\ L(a, \bigtriangledown) & L(a, \star) \end{bmatrix}$. Then, we use $\mathcal{X}_\phi^{a,\circ}$ to predict $\mathcal{X}_\phi^{a,\star}$ with a linear model

$$\mathcal{X}_\phi^{a,\star} = \beta + \mathcal{X}_\phi^{a,\circ} A + \varepsilon, \quad (27)$$

where A denotes the regression coefficient matrix, β is a constant vector, and ε measures regression residuals. Meanwhile, we can also use $\mathcal{X}_\phi^{a,\circ}$ and \mathcal{X}_ϕ^b to predict $\mathcal{X}_\phi^{a,\star}$

$$\mathcal{X}_\phi^{a,\star} = \beta' + (\mathcal{X}_\phi^{a,\circ} \oplus \mathcal{X}_\phi^b) A' + \varepsilon', \quad (28)$$

where we have applied notion \oplus to denote the concatenation of two vectors, i.e., $\mathcal{X}_\phi^{a,\circ} \oplus \mathcal{X}_\phi^b = (X_\phi^a(1), \dots, X_\phi^a(k), X_\phi^b(1), \dots, X_\phi^b(n))$ (see **Fig. 4**). According to Refs. [96, 97], the ordinary least squares regression for Eqs. (27-28) is suggested to minimize the determinant of covariance matrix of residuals (referred to as the generalized variance). The covariance matrices of residuals for Eqs. (27-28) are

$$\Sigma(\varepsilon) = \Sigma(\mathcal{X}_\phi^{a,\star} | \mathcal{X}_\phi^{a,\circ}), \quad (29)$$

$$\Sigma(\varepsilon') = \Sigma(\mathcal{X}_\phi^{a,\star} | \mathcal{X}_\phi^{a,\circ} \oplus \mathcal{X}_\phi^b). \quad (30)$$

The Granger causality can be defined as the natural logarithmic ratio between the determinant values of Eqs. (29-30) [96]

$$\mathcal{T}_G(\mathcal{X}_\phi^b \rightarrow \mathcal{X}_\phi^a) = \left\langle \ln \left[\frac{\det(\Sigma(\varepsilon))}{\det(\Sigma(\varepsilon'))} \right] \right\rangle, \quad (31)$$

where the average $\langle \cdot \rangle$ is implemented across multiple randomly generated configurations of $\mathcal{X}_\phi^{a,\star}$ and $\mathcal{X}_\phi^{a,\circ}$ (i.e., we

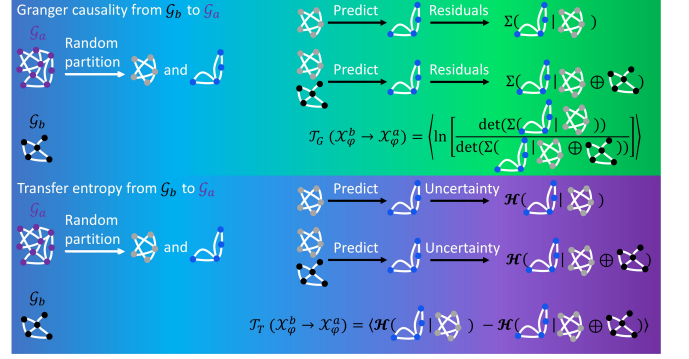


FIG. 4. Conceptual illustrations of Granger causality and transfer entropy between complex networks. To quantify the causal effects from network \mathcal{G}_b to network \mathcal{G}_a , we first do random partition on network \mathcal{G}_b to obtain two sub-networks. Then we predict the topology properties of one sub-network based on another sub-network. The prediction may involve with residuals (in terms of Granger causality) or uncertainty (in terms of transfer entropy). The causal effects from network \mathcal{G}_b to network \mathcal{G}_a are reflected by the reduction of residuals and uncertainty after we include the information of \mathcal{G}_b into the prediction. By repeating random partition and prediction, we can measure Granger causality and transfer entropy in terms of the average reduction of residuals and uncertainty.

can randomly select h configurations of $\mathcal{X}_\phi^{a,\star}$ and $\mathcal{X}_\phi^{a,\circ}$ to calculate h values of $\ln \left[\frac{\Sigma(\varepsilon)}{\Sigma(\varepsilon')} \right]$ and average across them to derive Eq. (31)). Please see **Fig. 4** for illustrations. Because $\mathcal{X}_\phi^{a,\star}$ and $\mathcal{X}_\phi^{a,\circ}$ are jointly Gaussian [96, 97], we can readily derive

$$\Sigma(\varepsilon) = L(a, \circ) + \frac{1}{n}J - \left(L(a, \triangle) + \frac{1}{n}J \right) \times \left(L(a, \star) + \frac{1}{n}J \right)^{-1} \left(L(a, \bigtriangledown) + \frac{1}{n}J \right). \quad (32)$$

However, $\Sigma(\varepsilon')$ can not be analytically derived by the discrete Schrödinger operators of networks unless we relax conditions (e.g., let $\mathcal{X}_\phi^{a,\star}$, $\mathcal{X}_\phi^{a,\circ}$, and \mathcal{X}_ϕ^b be jointly Gaussian as well). Similar to the situation in Eq. (21), we suggest that one can generate samples of $\mathcal{X}_\phi^{a,\star}$, $\mathcal{X}_\phi^{a,\circ}$, and \mathcal{X}_ϕ^b by inverse transform sampling [81] to estimate $\Sigma(\varepsilon')$ in practice. For convenience, we usually write Eq. (31) as $\mathcal{T}_G(\mathcal{X}_\phi^b \rightarrow \mathcal{X}_\phi^a) = \langle \mathcal{T}_G(\mathcal{X}_\phi^b \rightarrow \mathcal{X}_\phi^a) \rangle$, where $\mathcal{T}_G(\mathcal{X}_\phi^b \rightarrow \mathcal{X}_\phi^a) = \ln \left[\frac{\det(\Sigma(\varepsilon))}{\det(\Sigma(\varepsilon'))} \right]$.

Then, we turn to defining transfer entropy. In general, we can formulate transfer entropy based on conditional mutual information [57] (see **Fig. 4**)

$$\mathcal{T}_T(\mathcal{X}_\phi^b \rightarrow \mathcal{X}_\phi^a) = \langle \mathcal{I}(\mathcal{X}_\phi^{a,\star}; \mathcal{X}_\phi^b | \mathcal{X}_\phi^{a,\circ}) \rangle \quad (33)$$

$$= \langle \mathcal{H}(\mathcal{X}_\phi^{a,\star} | \mathcal{X}_\phi^{a,\circ}) - \mathcal{H}(\mathcal{X}_\phi^{a,\star} | \mathcal{X}_\phi^{a,\circ} \oplus \mathcal{X}_\phi^b) \rangle. \quad (34)$$

Similar to Eq. (32), we can derive

$$\mathcal{H}(\mathcal{X}_\phi^{a,*} | \mathcal{X}_\phi^{a,o}) = \mathcal{H}(\mathcal{X}_\phi^{a,*} \oplus \mathcal{X}_\phi^{a,o}) - \mathcal{H}(\mathcal{X}_\phi^{a,o}), \quad (35)$$

$$= \frac{n-k}{2} + \frac{n-k}{2} \log(2\pi) \\ + \frac{1}{2} \log \left[\frac{\det(L(a) + \frac{1}{n}J)}{\det(L(a, o) + \frac{1}{n}J)} \right] \quad (36)$$

because $\mathcal{X}_\phi^{a,*}$ and $\mathcal{X}_\phi^{a,o}$ are jointly Gaussian. Similar to Eq. (21) and $\Sigma(\varepsilon')$, we can not derive a general expression of $\mathcal{H}(\mathcal{X}_\phi^{a,*} | \mathcal{X}_\phi^{a,o} \oplus \mathcal{X}_\phi^b) = \mathcal{H}(\mathcal{X}_\phi^a, \mathcal{X}_\phi^b) - \mathcal{H}(\mathcal{X}_\phi^{a,o} \oplus \mathcal{X}_\phi^b)$. In practice, we can resolve this challenge by inverse transform sampling [81] the Kozachenko-Leonenko estimator of Shannon entropy [82, 83]. For convenience, Eq. (34)) is usually written as $\mathcal{T}_T(\mathcal{X}_\phi^b \rightarrow \mathcal{X}_\phi^a) = \langle \mathcal{T}_t(\mathcal{X}_\phi^b \rightarrow \mathcal{X}_\phi^a) \rangle$, where we define $\mathcal{T}_t(\mathcal{X}_\phi^b \rightarrow \mathcal{X}_\phi^a) = \mathcal{I}(\mathcal{X}_\phi^{a,*}; \mathcal{X}_\phi^b | \mathcal{X}_\phi^{a,o})$.

Please note that the causality metrics considered here, such as $\mathcal{T}_G(\mathcal{X}_\phi^b \rightarrow \mathcal{X}_\phi^a)$ and $\mathcal{T}_T(\mathcal{X}_\phi^b \rightarrow \mathcal{X}_\phi^a)$, should be referred to as apparent causality metrics according to Ref. [98] (one can see similar apparent causality metrics for time series in Refs. [89–95, 99]). To derive complete causality metrics that reflect causal relations more precisely (e.g., enable \mathcal{T}_G and \mathcal{T}_T approximate causal information flow [100]), one need to consider $\mathcal{T}_G(\mathcal{X}_\phi^b \rightarrow \mathcal{X}_\phi^a | \mathcal{Y})$ and $\mathcal{T}_T(\mathcal{X}_\phi^b \rightarrow \mathcal{X}_\phi^a | \mathcal{Y})$ given a reference variable \mathcal{Y} . Because the details of introducing \mathcal{Y} have been comprehensively explored in Refs. [96, 98, 101, 102] and these details do not imply critical challenges for mathematical derivations, we no longer repeat their analyses here. One can combine Refs. [96, 98, 101, 102] and our framework to readily derive $\mathcal{T}_G(\mathcal{X}_\phi^b \rightarrow \mathcal{X}_\phi^a | \mathcal{Y})$ and $\mathcal{T}_T(\mathcal{X}_\phi^b \rightarrow \mathcal{X}_\phi^a | \mathcal{Y})$ between networks.

V. GENERALIZATION OF ANALYTIC METRICS

One may notice that our derivations of all analytic metrics in Sec. IV are shown in a special case where \mathcal{X}_ϕ^a and \mathcal{X}_ϕ^b are both n -dimensional, meaning that networks \mathcal{G}_a and \mathcal{G}_b both contain n nodes. This limitation arises from the fact that we need to calculate $(L^\dagger(b) + \frac{1}{n}J)(L(a) + \frac{1}{n}J)$ in information divergence. The definitions of mutual information, Fisher information, Granger causality, and transfer entropy have no such a limitation and are generally applicable to arbitrary cases.

In practice, we frequently need to analyze relations between complex networks with distinct sizes (number of nodes). To make our information divergence applicable to these networks, we suggest a practical solution based

on Laplacian energy. Let us consider a case where \mathcal{X}_ϕ^a and \mathcal{X}_ϕ^b are m -dimensional and n -dimensional, respectively. Without loss of generality, we primarily discuss the case where $m > n$. The Laplacian energy of network \mathcal{G}_a (V_a, E_a) is defined as [103–106]

$$\mathcal{L}(\mathcal{G}_a) = \sum_{i=1}^m \lambda_i^2 = \sum_{i=1}^m \deg(v_i)^2 + \sum_{j \neq i} W_{ij}^2(a), \quad (37)$$

where $(\lambda_1, \dots, \lambda_m)$ are eigenvalues of $L(a)$ and $W(a)$ denotes the weighted adjacent matrix of \mathcal{G}_a . Note that $\deg(v_i) = \sum_{j=1}^n W_{ij}$. Based on Eq. (37), we can measure the importance of each node v_i in maintaining topology properties of \mathcal{G}_a by Laplacian centrality [104, 106]

$$\mathcal{A}(v_i, \mathcal{G}_a) = \frac{\mathcal{L}(\mathcal{G}_a) - \mathcal{L}(\mathcal{G}_a/\{v_i\})}{\mathcal{L}(\mathcal{G}_a)}, \quad (38)$$

where $\mathcal{G}_a/\{v_i\}$ means deleting node v_i from network \mathcal{G}_a . Note that we have $\mathcal{L}(\mathcal{G}_a) \geq \mathcal{L}(\mathcal{G}_a/\{v_i\})$, where the equality holds if and only if v_i is an isolate node (has no influence on main topology properties of \mathcal{G}_a) [104, 106]. In general, the Laplacian centrality of node v_i is determined by the number of walks it participates in \mathcal{G}_a , i.e., the number of closed walks (v_i, \dots, v_i) , the number of non-closed walks (v_i, \dots) and (\dots, v_i) where v_i is one of the end nodes, the number of non-closed walks (\dots, v_i, \dots) containing v_i as a middle node. In Ref. [106], it is suggested that Eq. (38) can be reformulated by analyzing

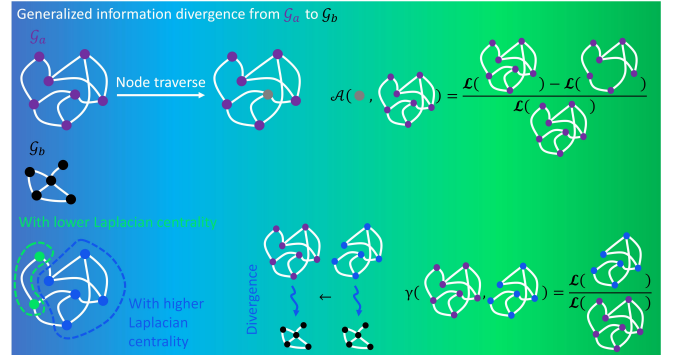


FIG. 5. Conceptual illustrations of the generalization of information divergence. When networks \mathcal{G}_a and \mathcal{G}_b have different sizes (e.g., network \mathcal{G}_a contains more nodes), the information divergence defined in Eq. (20) can not be calculated directly. Consequently, we need to measure the importance of nodes in \mathcal{G}_a from the perspective of network topology. In Eq. (38), we introduce $\mathcal{A}(\cdot, \mathcal{G}_a)$, the importance measurement based on Laplacian energy, as a possible approach. After assigning the importance of each node in \mathcal{G}_a , we can exclude the nodes with relatively lower importance to make the filtered \mathcal{G}_a have the same size as \mathcal{G}_b . Information divergence from the filtered \mathcal{G}_a to \mathcal{G}_b can be measured and treated as an approximation of the information divergence from the original \mathcal{G}_a to \mathcal{G}_b . The rationality γ of this approximation can be measured as the fraction of the lost Laplacian energy in the original Laplacian energy.

walks of length 2 (contain 3 nodes). Specifically, one can derive Eq. (39) following Ref. [106]

$$\mathcal{L}(\mathcal{G}_a) - \mathcal{L}(\mathcal{G}_a/\{v_i\}) = 4\eta_c(v_i) + 2\eta_e(v_i) + 2\eta_m(v_i), \quad (39)$$

where $\eta_c(v_i)$ measures the number of closed walks (v_i, v_j, v_i) , $\eta_e(v_i)$ measures the number of non-closed walks (v_i, v_j, v_k) and (v_j, v_k, v_i) , $\eta_m(v_i)$ measures the number of non-closed walks (v_j, v_i, v_k) . Applying the weight adjacent matrices $W(a)$ and $M(a)$ (here $M(a)$ is the weight adjacent matrix of network $\mathcal{G}_a/\{v_i\}$), we suggest that Eq. (39) can be readily calculated by Eq. (40)

$$\begin{aligned} & \mathcal{L}(\mathcal{G}_a) - \mathcal{L}(\mathcal{G}_a/\{v_i\}) \\ &= 4 \left[W(a)^2 \right]_{ii} + 2 \left[\sum_{j \neq k} \left[W(a)^2 \right]_{jk} - \sum_{j \neq k} \left[M(a)^2 \right]_{jk} \right]. \end{aligned} \quad (40)$$

Note that $\left[W(a)^2 \right]_{jk} = [W(a)W(a)]_{jk}$, the (i, j) element in matrix $W(a)^2$, is not equivalent to $W_{ij}^2(a)$, the second power of (i, j) element in matrix $W(a)$. Combining Eqs. (37-38) and Eq. (40), we can measure the Laplacian centrality of each node in network \mathcal{G}_a and only keep n nodes with relatively large Laplacian centrality values. In other words, $m - n$ nodes are filtered because their effects on topology properties of \mathcal{G}_a are less significant (see **Fig. 5**). We refer to the network after filtering as $\hat{\mathcal{G}}_a$ and denote its Laplacian and Gaussian variable as $\hat{L}(a)$ and $\hat{\mathcal{X}}_\phi^a$, respectively. Then we can approximatively calculate information divergence in Eq. (20) by replacing $L(a)$ and \mathcal{X}_ϕ^a as $\hat{L}(a)$ and $\hat{\mathcal{X}}_\phi^a$ (see **Fig. 5**). In the case where $m < n$, we can similarly deal with network \mathcal{G}_b following the above approach.

The rationality γ of the above approximation can be measured based on the loss of Laplacian energy. Taking the case where $m > n$ as an instance, we define the rationality of approximating \mathcal{G}_a by $\hat{\mathcal{G}}_a$ as (see **Fig. 5**)

$$\gamma \left(\mathcal{L}(\mathcal{G}_a), \mathcal{L}(\hat{\mathcal{G}}_a) \right) = \frac{\mathcal{L}(\hat{\mathcal{G}}_a)}{\mathcal{L}(\mathcal{G}_a)}. \quad (41)$$

To this point, we have presented analytic metrics of network relations from the perspectives of encoding, decoding, and causal analyses in Sec. IV. We have also explored their possible generalization in Sec. V. Below, we validate our approach on representative complex networks to define encoding, decoding, and causal analysis tasks.

VI. ENCODING, DECODING, AND CAUSAL ANALYSES ON RANDOM NETWORK MODELS

We first consider encoding, decoding, and causal analyses on random network models, such as Watts-Strogatz

model (with small-world properties) [107], Erdos-Renyi model (each pair of nodes are connected according to a probability quantity) [108], and Barabási-Albert model (with scale-free properties) [109]. These random network models are important in statistical physics and mathematics (e.g., for analyzing percolation on small-world networks [110], Erdos-Renyi networks [111], and scale-free networks [112]). Meanwhile, they are prototypes in analyzing social [113, 114], biological [115–120], and chemical [121, 122] networks. Therefore, the encoding, decoding, and causal analyses implemented on these models can be further generalized to diverse real networks with corresponding topology properties. The main motivation of our analyses on random network models is to validate the proposed analytic metrics of network relations and suggest practical solutions of potential limitations.

A. The node deletion process

In **Fig. 6**, we implement encoding, decoding, and causal analyses during the node deletion process. In our experiment, a Watts-Strogatz model (each node originally connects with $\alpha = 15$ nodes, and edges are randomly re-wired according a probability of $\beta = 0.7$), an Erdos-Renyi model (each pair of nodes are connected according to a probability of $\rho = 0.15$), and a Barabási-Albert model (a connected network of $\kappa = 50$ nodes is set as the initialization seed) are generated and initially contain 300 nodes (see **Fig. 6a** for illustrations). Note that all the network parameters used in initialization are set for convenience, and our analyses do not critically rely on these parameters. The node deletion process consists of 200 iterations. In each iteration, we randomly delete one node and all related edges from these three networks. Encoding, decoding, and causal analyses are implemented between \mathcal{X}_ϕ^b , the networks in the n -th iteration ($n \in \mathbb{Z} \cap [1, 200]$) and \mathcal{X}_ϕ^a , the networks in their initialized forms. Certainly, one may notice that the decoding analysis has not been explicitly defined by the above settings. In real cases, the decoding analysis should be defined according to research demands. In our research, we present an instance of the decoding analysis based on a parameter vector $\Theta = (\theta_1, \dots, \theta_{10})$ controlled by \mathcal{X}_ϕ^b . Parameter vector Θ is designed to affect \mathcal{X}_ϕ^a and make it become $\mathcal{X}_\phi^a + \varepsilon$, where $\varepsilon \sim \mathcal{N}(\mathbf{0}, \Theta)$ denotes the effects of Θ on \mathcal{X}_ϕ^a . For convenience, we consider a case where Θ is defined as the degree vector ($\theta_1 = \deg(v_1), \dots, \theta_{10} = \deg(v_{10})$) of a set of nodes $\{v_1, \dots, v_{10}\}$ randomly selected from network \mathcal{G}_b . By repeating random sampling, we can obtain a set of observations $\{\Theta^i = (\theta_1^i, \dots, \theta_{10}^i)\}$ of the parameter vector, each of which corresponds to an effect on \mathcal{X}_ϕ^a to create an observation $\mathcal{X}_\phi^a + \varepsilon_i$. Based on these settings, the decoding analysis can be implemented to measure the information of Θ contained in the probability distribution of $\mathcal{X}_\phi^a + \varepsilon$.

As n increases, more topology properties are changed due to node deletion. Therefore, \mathcal{X}_ϕ^a and \mathcal{X}_ϕ^b are expected

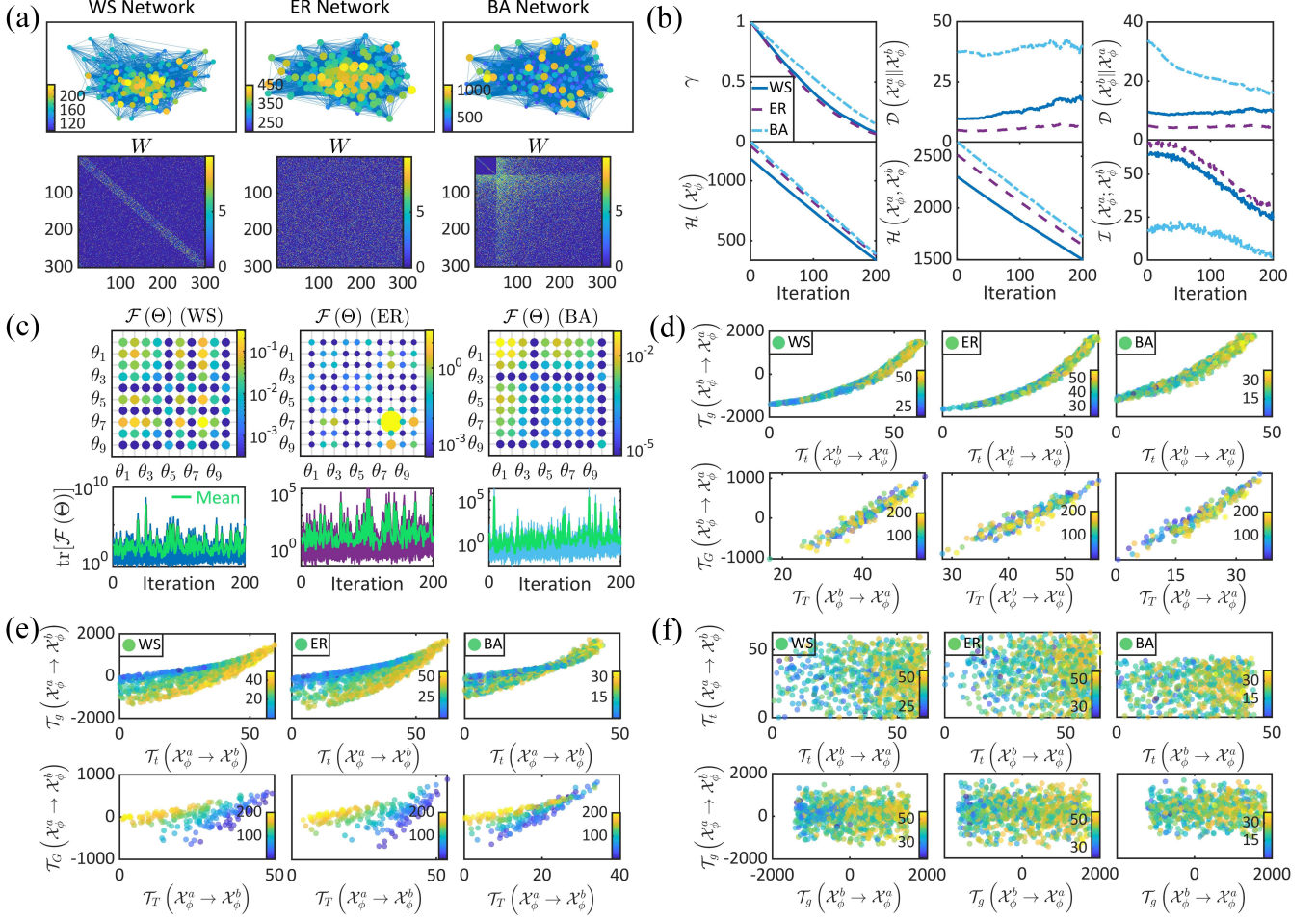


FIG. 6. Encoding, decoding, and causal analyses on random network models during node deletion processes. (a) Watts-Strogatz (WS), Erdos-Renyi (ER), and Barabási-Albert (BA) random networks and their adjacent matrices. (b) Variables used for network approximation and encoding analysis are shown as the functions of iterations. (c) Examples of Fisher information matrices in the first iteration are illustrated (upper parallel). Fisher information quantities, the traces of Fisher information matrices, are calculated in each iteration (deep blue, purple, and light blue lines in bottom parallel). Meanwhile, the mean Fisher information quantities, which are averaged across different Θ conditions, are also shown (green lines in bottom parallel). (d-e) Two causality metrics, Granger causality and transfer entropy, are positively correlated with each other for $X_\phi^b \rightarrow X_\phi^a$ or $X_\phi^a \rightarrow X_\phi^b$. (f) Causality metrics are asymmetric, i.e., Granger causality and transfer entropy for $X_\phi^b \rightarrow X_\phi^a$ are not correlated with those for $X_\phi^a \rightarrow X_\phi^b$.

to become increasingly different during node deletion. In **Fig. 6b**, the enlarging difference between X_ϕ^a and X_ϕ^b can be reflected by the decreasing mutual information and the slightly increasing information divergence from X_ϕ^a to X_ϕ^b . However, we also observe reductions in the information divergence from X_ϕ^b to X_ϕ^a . We hypothesize that the inconsistent variation trends of $\mathcal{D}(X_\phi^a \| X_\phi^b)$ and $\mathcal{D}(X_\phi^b \| X_\phi^a)$ may arise from the asymmetry properties of information divergence (i.e., information divergence is a kind of pseudo-distance because $\mathcal{D}(X_\phi^a \| X_\phi^b) \neq \mathcal{D}(X_\phi^b \| X_\phi^a)$). Meanwhile, the information divergence generalized by the Laplacian-energy-based approach in Sec. V may fail to reflect the actual divergence between

networks with different sizes. In real situations, we suggest one to tackle this problem by analyzing the mean value of $\mathcal{D}(X_\phi^a \| X_\phi^b)$ and $\mathcal{D}(X_\phi^b \| X_\phi^a)$. In **Fig. 6c**, we illustrate several instances of Fisher information matrices in our decoding analysis. Using the Fisher information matrices generated in each iteration, we can further calculate Fisher information quantities, the traces of Fisher information matrices, to reflect the decoding precision of X_ϕ^b from X_ϕ^a . In our experiments, the observations of decoding precision and their mean values persistently oscillate across different iterations. This phenomenon may arise from the randomness during the sampling of parameter vector Θ on network \mathcal{G}_b . In real situations, a more monotonous trend of Fisher information quantities may be observed if Θ is controlled by specific global prop-

	Direction	Variables	WS network	ER network	BA network	Statistical significance
Node deletion	$\mathcal{X}_\phi^b \rightarrow \mathcal{X}_\phi^a$	\mathcal{T}_g and \mathcal{T}_t	$R = 0.9608$	0.9614	0.9731	$p < 10^{-10}$
		\mathcal{T}_G and \mathcal{T}_T	$R = 0.9617$	0.9476	0.96	$p < 10^{-10}$
	$\mathcal{X}_\phi^a \rightarrow \mathcal{X}_\phi^b$	\mathcal{T}_g and \mathcal{T}_t	$R = 0.7960$	0.7756	0.9269	$p < 10^{-10}$
		\mathcal{T}_G and \mathcal{T}_T	$R = 0.4821$	0.5113	0.7942	$p < 10^{-10}$
Edge rewiring	$\mathcal{X}_\phi^b \rightarrow \mathcal{X}_\phi^a$	\mathcal{T}_g and \mathcal{T}_t	$R = 0.9672$	0.9355	0.9581	$p < 10^{-10}$
		\mathcal{T}_G and \mathcal{T}_T	$R = 0.9497$	0.7118	0.8568	$p < 10^{-10}$
	$\mathcal{X}_\phi^a \rightarrow \mathcal{X}_\phi^b$	\mathcal{T}_g and \mathcal{T}_t	$R = 0.9618$	0.6834	0.9641	$p < 10^{-10}$
		\mathcal{T}_G and \mathcal{T}_T	$R = 0.9145$	0.3809	0.9618	$p < 10^{-10}$
Node adding	$\mathcal{X}_\phi^b \rightarrow \mathcal{X}_\phi^a$	\mathcal{T}_g and \mathcal{T}_t	$R = 0.6996$	0.7362	0.7116	$p < 10^{-10}$
		\mathcal{T}_G and \mathcal{T}_T	$R = 0.3229$	0.3599	0.3409	$p < 10^{-10}$
	$\mathcal{X}_\phi^a \rightarrow \mathcal{X}_\phi^b$	\mathcal{T}_g and \mathcal{T}_t	$R = 0.8816$	0.8911	0.8161	$p < 10^{-10}$
		\mathcal{T}_G and \mathcal{T}_T	$R = 0.7893$	0.8105	0.7447	$p < 10^{-10}$

TABLE I. Correlation R between Granger causality and transfer entropy on Watts-Strogatz (WS), Erdos-Renyi (ER), and Barabási-Albert (BA) random networks.

erties of network \mathcal{G}_b . In **Fig. 6d-e**, we demonstrate that our proposed causality metrics, Granger causality and transfer entropy, are positively correlated with each other. In the direction of $\mathcal{X}_\phi^b \rightarrow \mathcal{X}_\phi^a$, we calculate 10 pairs of $\mathcal{T}_g(\mathcal{X}_\phi^b \rightarrow \mathcal{X}_\phi^a)$ and $\mathcal{T}_t(\mathcal{X}_\phi^b \rightarrow \mathcal{X}_\phi^a)$ in each iteration, whose mean values are the corresponding Granger causality $\mathcal{T}_G(\mathcal{X}_\phi^b \rightarrow \mathcal{X}_\phi^a)$ and transfer entropy $\mathcal{T}_T(\mathcal{X}_\phi^b \rightarrow \mathcal{X}_\phi^a)$. The positive correlations between $\mathcal{T}_g(\mathcal{X}_\phi^b \rightarrow \mathcal{X}_\phi^a)$ and $\mathcal{T}_t(\mathcal{X}_\phi^b \rightarrow \mathcal{X}_\phi^a)$ (they are analyzed in pairs) on three random network models and the positive correlations $\mathcal{T}_G(\mathcal{X}_\phi^b \rightarrow \mathcal{X}_\phi^a)$ and $\mathcal{T}_T(\mathcal{X}_\phi^b \rightarrow \mathcal{X}_\phi^a)$ on three models are shown in **Table 1** and **Fig. 6d**, which turn out to be significantly strong. Similarly, we implement the same correlation analysis in the direction of $\mathcal{X}_\phi^a \rightarrow \mathcal{X}_\phi^b$. The positive correlations between corresponding variables on three models are relatively strong as well (see **Table 1** and **Fig. 6e**). Meanwhile, we show that there exists no significant correlation between the causality measured in the direction of $\mathcal{X}_\phi^a \rightarrow \mathcal{X}_\phi^b$ and that measured in the direction of $\mathcal{X}_\phi^b \rightarrow \mathcal{X}_\phi^a$ because causality is generally asymmetric (see **Fig. 6f**). These results demonstrate the validity of our proposed analytic network relation metrics.

B. The rewiring process

One may reasonably suspect that the reduction of mutual information in **Fig. 6** is caused by the decreasing dimension number of \mathcal{X}_ϕ^b rather than the enlarging difference between \mathcal{X}_ϕ^a and \mathcal{X}_ϕ^b . To disprove this possibility, we replace the node adding process by a rewiring process. All the settings used for random network initialization keep the same as those in **Fig. 6**. After the initialization, we randomly select one node and rewire its edges in each iteration. The edge rewiring rules can be set in diverse forms but should be different from the edge wiring rules in original random networks (e.g., the rewiring rules in the Barabási-Albert random network should not be preferential attachment). Otherwise, the generated network after rewiring may not become increasingly different from the original one as the iteration number n increases. To ensure the enlarging difference, we define the rewiring processes of initialized Watts-Strogatz, Erdos-Renyi, and Barabási-Albert random networks following the wiring rules of Erdos-Renyi ($\rho = 0.5$), Watts-Strogatz ($\alpha = 40$ and $\beta = 0.1$), and Erdos-Renyi ($\rho = 0.5$) models, respectively. Please see Sec. VI A for the precise meaning of parameters ρ , α , and β . Note that our rewiring rules are set only for convenience. One can consider other settings in practice. During the rewiring process, we follow

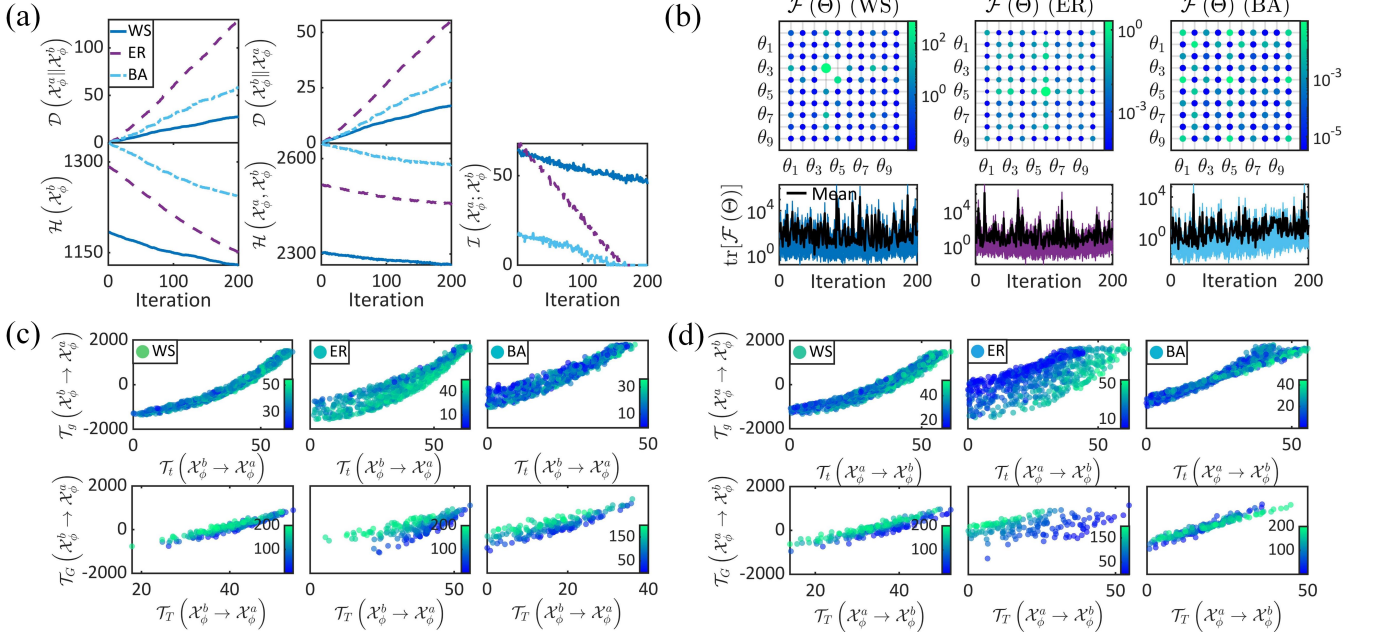


FIG. 7. Encoding, decoding, and causal analyses on random network models during rewiring processes. (a) Variables used in encoding analysis are shown as the functions of iterations. Note that γ , the rationality of network approximation, is not shown since it is constant during rewiring. (b) Examples of Fisher information matrices in the first iteration are illustrated in the upper parallel. Fisher information quantities (deep blue, purple, and light blue lines) and their mean values averaged across different Θ conditions (black lines) are shown in the bottom parallel. (c-d) The positive correlations between Granger causality and transfer entropy are shown.

the same idea described in Sec. VI A to define encoding, decoding, and causal analyses between the original networks, \mathcal{X}_ϕ^a , and the generated networks after each time of rewiring, \mathcal{X}_ϕ^b .

In **Fig. 7**, the results of encoding, decoding, and causal analyses are shown. During rewiring processes, we can see the decreasing mutual information and the increasing information divergence (in both directions), which keeps consistency with the enlarging difference between \mathcal{X}_ϕ^a and \mathcal{X}_ϕ^b (see **Fig. 7a**). In **Fig. 7b**, we present the instances of Fisher information matrices, based on which, we can further calculate Fisher information quantities to measure the decoding precision of \mathcal{X}_ϕ^b from \mathcal{X}_ϕ^a . Similar to the situation in **Fig. 6c**, the observations of decoding precision and their mean quantities oscillate due to the random sampling effects on parameter vector Θ . In **Fig. 7c-d** and **Table 1**, we can see the strong positive correlations between Granger causality and transfer entropy in the direction of $\mathcal{X}_\phi^b \rightarrow \mathcal{X}_\phi^a$ and in the direction of $\mathcal{X}_\phi^a \rightarrow \mathcal{X}_\phi^b$. All these results suggest that our observations in **Fig. 6** are not coincidentally caused by the decreasing dimension number of \mathcal{X}_ϕ^b since the rewiring process does not change the network size.

C. The node adding process

Certainly, one may still doubt whether the decreasing mutual information in **Figs. 6-7** is coincidentally caused

by the decreasing Shannon entropy of \mathcal{X}_ϕ^b . To disprove this possibility, we replace the rewiring process in **Fig. 7** by the node adding process to re-conduct our encoding, decoding, and causal analyses. Similar to the rewiring process, the node adding process is designed to ensure the enlarging difference between the original networks, \mathcal{X}_ϕ^a , and the generated networks after each time of node adding, \mathcal{X}_ϕ^b as well. Specifically, we add a node in each iteration and connect it with existing nodes according to certain wiring rules. The wiring rules are set to be distinct from those in the original networks. For convenience, we design the wiring of added nodes in initialized Watts-Strogatz, Erdos-Renyi, and Barabási-Albert networks following the rules in Erdos-Renyi ($\rho = 0.5$), Watts-Strogatz ($\alpha = 40$ and $\beta = 0.1$), and Erdos-Renyi ($\rho = 0.5$) models, respectively.

In **Fig. 8**, we present the results of encoding, decoding, and causal analyses during node adding processes. One can see that the decreasing mutual information and the increasing information divergence (in both directions) coexist with the increasing Shannon entropy of \mathcal{X}_ϕ^b (**Fig. 8a**). These results disprove the possible validity issues concerned above. The decoding analysis results are shown in **Fig. 8b** while the causal analysis results are illustrated in **Fig. 8c-d** and **Table 1**. Because these results are presented in the same form as **Figs. 6-7**, here we no longer discuss them in details.

To this point, we have validated our encoding, decoding, and causal analyses on representative random net-

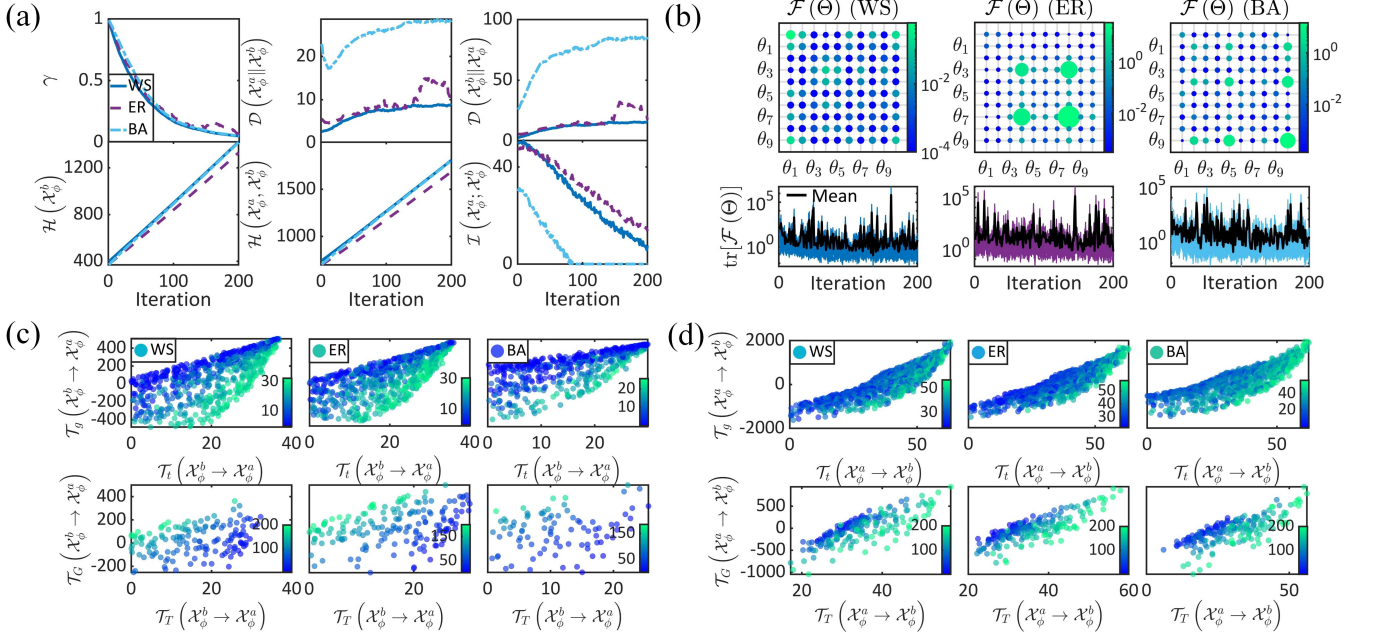


FIG. 8. Encoding, decoding, and causal analyses on random network models during node adding processes. (a) Variables used for network approximation and encoding analysis are presented as the functions of iterations. (b) Examples of Fisher information matrices in the first iteration (upper parallel), Fisher information quantities (deep blue, purple, and light blue lines in the bottom parallel), and mean Fisher information quantities averaged across different Θ conditions (black lines in the bottom parallel) are illustrated. (c-d) The positive correlations between Granger causality and transfer entropy are suggested.

work models. Our proposed network relation metrics are principally suggest as able to reflect the difference between complex networks. Although some limitations of these metrics are observed in our experiments (e.g., information divergence quantities measured in different directions may have inconsistent variation trends), there exist potential tricks to deal with them (e.g., average all the asymmetric network relation metrics across the direction of $\mathcal{X}_\phi^b \rightarrow \mathcal{X}_\phi^a$ and the direction of $\mathcal{X}_\phi^a \rightarrow \mathcal{X}_\phi^b$). Below, we apply our theory on real complex networks with these tricks. We show how our theory may promote the analyses of protein network (a node similarity analysis task) and chemical compound networks (a network similarity analysis task).

VII. ENCODING, DECODING, AND CAUSAL ANALYSES ON REAL NETWORKS

Among various fundamental tasks in network analysis, assigning node similarity in a given network and measuring network similarity in network ensembles are two important ones, which are closely related to node classification and network classification tasks in machine learning. Here we implemented these two kinds of similarity measurement tasks under our theoretical framework, respectively.

A. The analysis of protein network

The data set used for node similarity measurement is a protein-protein interaction network [123]. In the network, nodes (there are 2361 nodes of 13 types) correspond to proteins and edges (7182 edges in total) represent protein-protein interactions in the yeast [123]. To apply our theory in node similarity analysis, we need to first represent each node by a sub-network consisting of this node, its neighbors, and all relevant edges. To ensure the quality of such a representation, we primarily focus on the nodes with more than 5 neighbors. Then, we measure similarity between these nodes by implementing encoding, decoding, and causal analyses between their corresponding sub-networks. The decoding analysis is implemented under the same framework used in Sec. VI, where we set the parameter vector as $\Theta = (\theta_1, \dots, \theta_3)$ (the vector length of Θ is set as smaller than the minimum size of node representation to support random sampling). To avoid the influence of the potential inconsistent variation trends of asymmetric network relation metrics in different directions (similarity should be symmetric), we average information divergence, Fisher information, Granger causality, and transfer entropy across the direction of $\mathcal{X}_\phi^b \rightarrow \mathcal{X}_\phi^a$ and the direction of $\mathcal{X}_\phi^a \rightarrow \mathcal{X}_\phi^b$ to make them non-directional.

In **Fig. 9a**, we first illustrate the original protein-protein interaction network. As one of the explored applications, we measure the node importance in term of the closeness [124, 125] constrained by non-directional

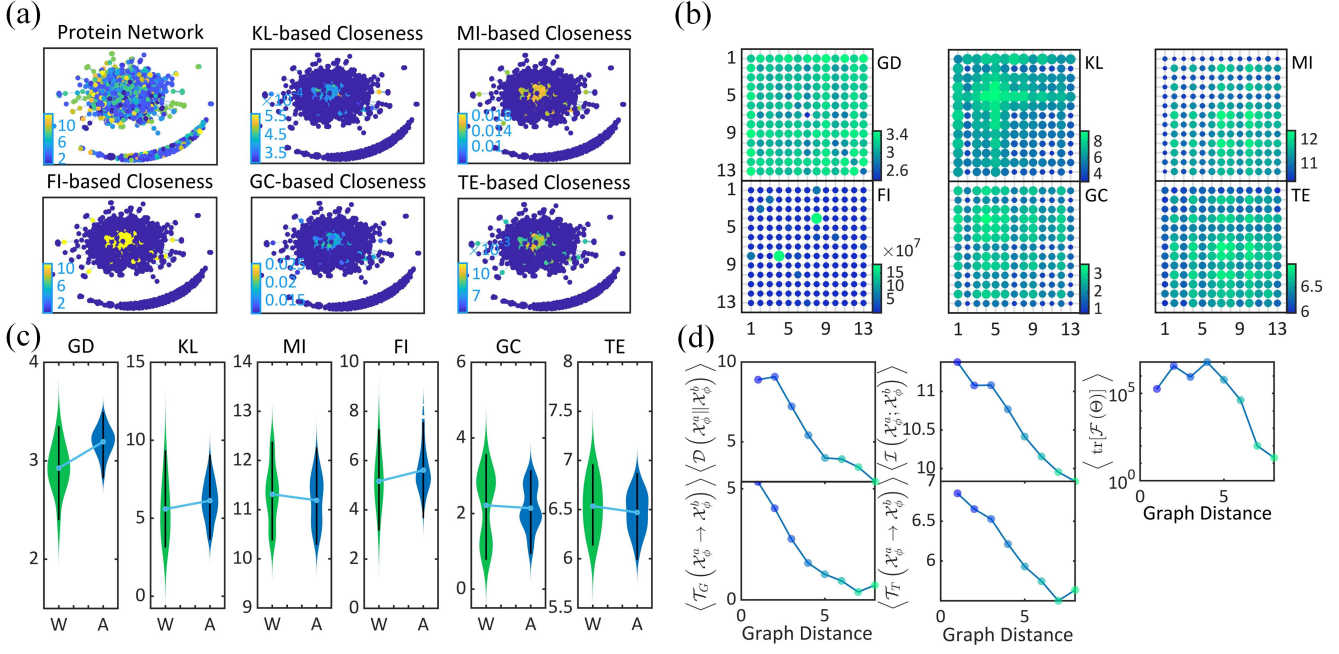


FIG. 9. Encoding, decoding, and causal analyses on a protein network. Encoding, decoding, and causal analyses are only implemented among the nodes with no less than five neighbors. Except for mutual information, the other variables are averaged between two analysis directions (i.e., averaged between $\mathcal{X}_\phi^b \rightarrow \mathcal{X}_\phi^a$ and $\mathcal{X}_\phi^a \rightarrow \mathcal{X}_\phi^b$) to make them non-directional. (a) The network of 13 types of proteins is presented (the first network in the upper parallel). Based on these non-directional encoding, decoding, and causal analyses results, the constrained node centrality (e.g., the closeness) is measured on the nodes with more than 5 neighbors. Specifically, the costs of edge traversal are assigned according to the information divergence (KL) as well as the inverses of the mutual information (MI), Fisher information quantity (FI), Granger causality (GC), and transfer entropy (TE), to measure the constrained closeness on these nodes. As for the nodes with no more than 5 neighbors, their centrality values are assigned as the minimum value of constrained closeness. The derived constrained node centrality distributions are shown, in which the colors of nodes are defined by their closeness quantities. (b) The mean graph distance (GD), KL, MI, FI, GC, and TE averaged within a protein class or across two different classes. (c) The mean GD, KL, MI, FI, GC, and TE averaged within a protein class (W) or across two protein classes (A) are compared in the violin plots, in which blue lines indicate the variation of expectation values. (d) The variables used in encoding, decoding, and causal analyses are shown as the functions of graph distance.

encoding, decoding, and causality metrics (the constraint is realized by assigning the costs of edge traversal according to these metrics). The spatial distributions of constrained closeness are shown in **Fig. 9a**, which may be considered as the reflection of node importance from the perspectives of encoding, decoding, and causality in future explorations. Given our proposed network relation metrics, our primary motivation is to verify if they can reflect the category relations between different nodes, i.e., whether two nodes correspond to the same type of protein. Because the neighbouring relations represent protein-protein interactions in the yeast, the graph distance (the length of the shortest path between two nodes) can naturally reflect the difference between proteins. Therefore, we also include the graph distance in our analysis. In **Fig. 9b**, we calculate the mean graph distance, encoding, decoding, and causality metrics averaged within a protein class or across two different classes. Based on these results, we can further compare the mean values of the graph distance and our proposed network relation metrics within the same class or across different

classes. As **Fig. 9c** suggests, most of the analyzed variables can correctly reflect the fact that the proteins from distinct classes have larger difference (e.g., the average mutual information quantities between the proteins from the same class are larger than those between the proteins from different classes). The only one exception is the Fisher information quantity calculated under the preset decoding framework because the defined parameter vector Θ may not establish an informative decoding relation between \mathcal{X}_ϕ^a and \mathcal{X}_ϕ^b . In **Fig. 9d**, we represent the averaged quantities of encoding, decoding, and causality variables as the functions of graph distance. All variables are observed to decrease as the graph distance increases. Except for information divergence, the variation trends of other variables suggest their capacities to reflect the decreasing similarity between the proteins with a larger graph distance. As for information divergence, its averaged quantities decrease with the graph distance because extremely large information divergence quantities may coexist with small graph distance values within a class (e.g., class 5 in **Fig. 9b**). Although infor-

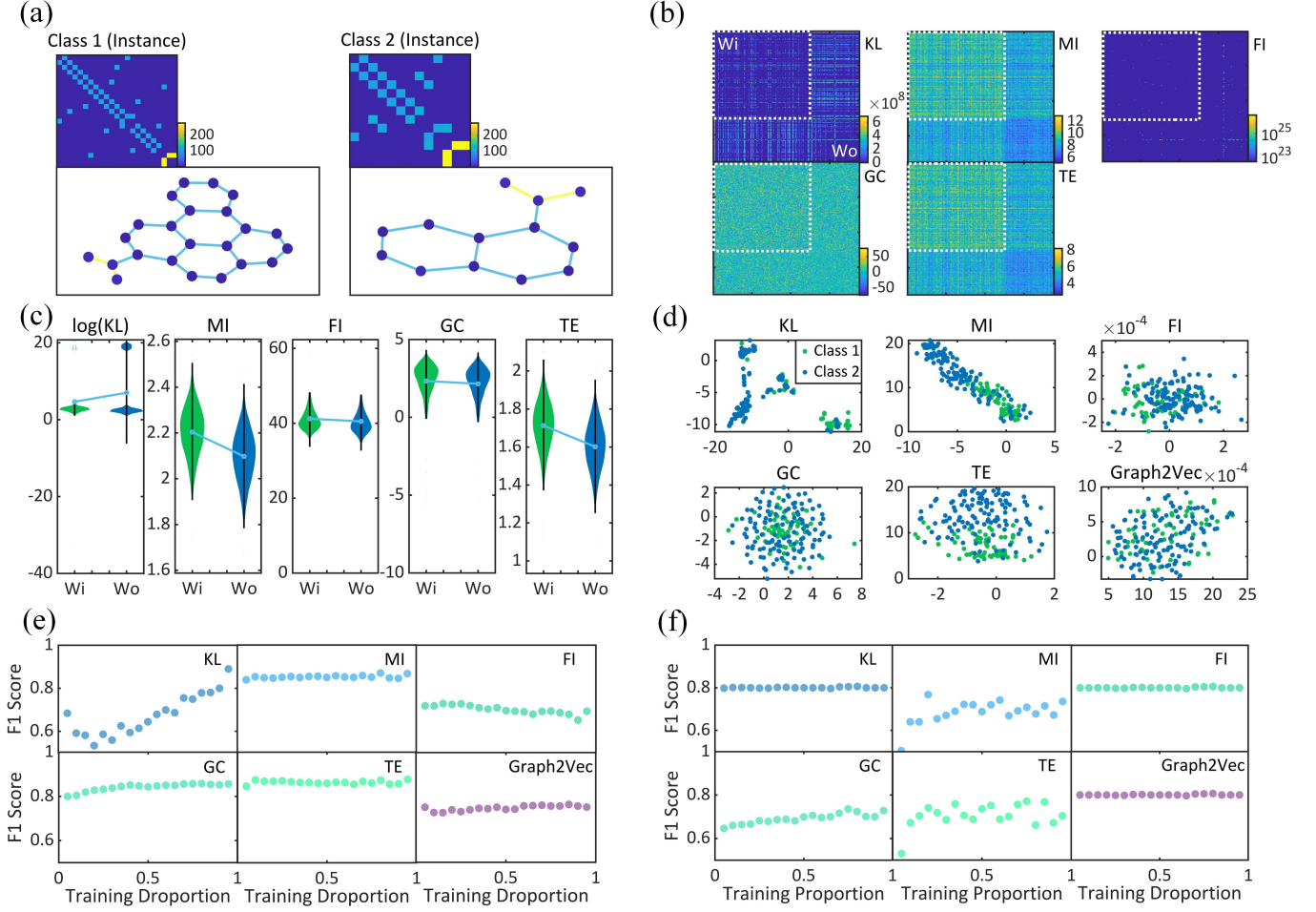


FIG. 10. Encoding, decoding, and causal analyses on chemical compound networks. (a) Two instances of the chemical compounds selected from different classes are presented, where the weighted adjacent matrices (upper parallel) and the corresponding topology structures (bottom parallel) are illustrated. Note that edges are colored according to chemical bond labels. (b) The matrices of non-directional encoding, decoding, and causal analyses results among all chemical compounds. Specifically, the encoding, decoding, and causal relations among the first class of chemical compounds are surrounded by white dotted boxes (marked as “Wi”). Those relations among the second class of chemical compounds as well as those relations between the first and the second classes of chemical compounds are outside of white dotted boxes (marked as “Wo”). (c) The mean KL, MI, FI, GC, and TE averaged within “Wi” or within “Wo” are compared in the violin plots, in which blue lines indicate the variation of expectation values. Note that the mean KL is shown in a logarithmic plot. (d) The t-SNE analyses are implemented based on the non-directional encoding, decoding, causal, and Graph2Vec analyses results in (b). (e-f) The assessment results of classification performance of a naive Bayes classifier and a logistic classifier are shown as the functions of training proportion, i.e., the proportion of training data among all the data, to show the robustness of performance.

mation divergence principally reflects the difference between proteins (e.g., see Fig. 9c), it fails on concrete protein classes (e.g., class 5).

In sum, we have suggested that our encoding, decoding, and causal analyses may principally support the measurement of node similarity on a protein-protein interaction network. Nevertheless, some proposed network relation metrics (e.g., information divergence) may fail to correctly reflect the within-class and cross-class differences of specific proteins, which remain as limitations for future explorations.

B. The analysis of chemical compound networks

The data used for network similarity measurement is a collection of mutagenic aromatic and heteroaromatic nitro compounds (188 compounds in total) [126]. Each chemical compound is represented by a network of atoms and is classified into two classes according to their mutagenic effects on specific gram negative bacteria [126]. The first class includes all the chemical compounds with mutagenic effects while the second class consists of the chemical compounds without mutagenic effects. To reflect the chemical properties of each compound \mathcal{X}_ϕ^a , we

define its weighted adjacent matrix as

$$W_{i,j}(a) = \beta_i \beta_j + \xi_{i,j}, \quad (42)$$

where β_i denotes the label of atom i and $\xi_{i,j}$ denotes the label of chemical bond between atoms i and j . Based on this definition, we conduct encoding, decoding, and causal analyses between chemical compounds to measure their similarity. Specifically, the decoding analysis is implemented following the same way described in Sec. VI, where the parameter vector is set as $\Theta = (\theta_1, \dots, \theta_{15})$.

In **Fig. 10a**, we show several instances from two chemical compound classes. According to the definition of these two classes, it is expected that the first class of chemical compounds have higher similarity with each other because they all have similar mutagenic effects on gram negative bacteria. As for the second class of chemical compounds, we naturally speculate that they have lower within-class and cross-class similarities because there may exist various factors to make them irrelevant to gram negative bacteria (the diversity of chemical compounds in the second class is higher). **Fig. 10b-c** present the results of encoding, decoding, and causal analyses to reflect the similarity between chemical compounds (all asymmetric network relation metrics are averaged across the direction of $\mathcal{X}_\phi^b \rightarrow \mathcal{X}_\phi^a$ and the direction of $\mathcal{X}_\phi^a \rightarrow \mathcal{X}_\phi^b$). We discover that information divergence quantities calculated within the first class are smaller than those calculated in other situations. Other network relation variables are consistently larger when they are calculated within the first class. These results generally validate the above speculations and suggest the possibility to distinguish between these two chemical compound classes based on our proposed theory. To demonstrate this possibility, we first implement the *t*-SNE analysis [127], a kind of unsupervised machine learning approach, on the matrices shown in **Fig. 10b**. We treat each raw of these matrices as a feature vector of the corresponding chemical compound, based on which we can embed the compound into a space with high data separability. For comparison, we also provide the *t*-SNE results of the feature vectors generated by the Graph2Vec framework, a graph representation learning approach (note that we set the feature vector length as 32) [31]. **Fig. 10d** presents our *t*-SNE analysis results, where two classes of chemical compounds generally form two separable clusters after embedding. Some embedding results based on our theory have better separability than those obtained from the Graph2Vec. In **Fig. 10e-f**, we further conduct supervised machine learning tasks on the feature vectors defined above to classify chemical compounds. Based on the results of encoding, decoding, and causal analyses, even simple learners such as a naive Bayes classifier (**Fig. 10e**) and a logistic classifier (**Fig. 10f**) can achieve high and robust learning performance (measured by the F1 score) on the task originally prepared for advanced embedding frameworks (e.g., the Graph2Vec [31] or learners (e.g., graph neural networks [128]).

In sum, we have realized the similarity analysis of com-

plex chemical compounds by our encoding, decoding, and causal analyses, which further supports machine learning tasks on chemical compounds with ideal performance.

VIII. DISCUSSION

A. Summary of our work

In this paper, we have introduced a possible way to measure analytic relations between complex networks. Our theory explores a mapping ϕ to map an arbitrary network $\mathcal{G}(V, E)$ to a random variable \mathcal{X}_ϕ distributed on node set V . The random variable is defined as $\mathcal{X}_\phi \sim \mathcal{N}(\mathbf{0}, L + \frac{1}{n}J)$, a Gaussian variable characterized by a function of the discrete Schrödinger operator L (or referred to as the combinatorial graph Laplacian) of network \mathcal{G} . On the one hand, such a definition ensures that the average smoothness of mapping ϕ on network \mathcal{G} is fully determined by the information of network topology properties contained in discrete Schrödinger operator L . On the other hand, this definition satisfies the requirements of maximum entropy property of variable \mathcal{X}_ϕ to promote the applicability in measuring information quantities. In Sec. VIII C, we shall suggest a dual definition of $\mathcal{X}_\phi \sim \mathcal{N}(\mathbf{0}, L + \frac{1}{n}J)$ and discuss their differences from the perspective of network representation.

Based on the proposed \mathcal{X}_ϕ , we further define encoding (information divergence and mutual information), decoding (Fisher information), and causal analyses (Granger causality and transfer entropy) between any pair of complex networks. We have validated these analyses on random network models (node deletion, edge rewiring, and node adding processes), protein-protein interaction network, and chemical compound network ensembles, suggesting their abilities to analytically measure network similarity and robustly promote network classification tasks.

An open-source release of our algorithms can be seen in Ref. [59].

B. Progress compared with previous works

Although mainstream network relation analysis approaches developed in computer science, such as embedding- [30, 32], matching- [33–35], and kernel-based [36, 37] methods, have been extensively applied in various science and engineering fields (e.g., in neuroscience [37, 49–51]), these approaches either suffer from the high computational complexity (e.g., matching-based [33]) or the dependence on empirical choice of network features (e.g., embedding-based [30]) and kernel functions (e.g., kernel-based [48]). Most importantly, these approaches do not present explicit and analytic expressions of universal network relations. Consequently, they are not applicable to developing mathematics and statistical physics theories of complex networks, as theoretical

derivations usually require analytic and explainable definitions rather than numerical solutions.

Compared with previous works, the main progress accomplished in our research is to suggest a general way to represent the topology properties of an arbitrary network by a Gaussian variable characterized by the function of the discrete Schrödinger operator L . The effectiveness of such a representation has been demonstrated by our experiments on random network models and real networks. We notice that similar ideas can be seen in several studies of graph signal, where researchers apply factor analysis [78] and low-rank models [79, 80] to suggest that graph Laplacian learning can be promoted by a Gaussian Markov random field representation defined whose covariance matrix as $\Sigma = L^\dagger$ [76, 77]. Recently, such an idea has been applied in solving graph optimal transport problems to support graph comparison and classification [53, 129]. The difference between these previous studies [53, 76, 77, 129] and our work lies in that they pre-set the covariance matrix of Gaussian variable as $\Sigma = L^\dagger$ while we make progress in analytically deriving $\Sigma = L + \frac{1}{n}J$ according to smoothness and maximum entropy properties (see Sec. VIII C for a mathematical analysis of the difference). As suggested by Sec. III, our derived results make the covariance matrix invertible, ensuring the possibility to calculate numerous quantities defined with Σ^{-1} in Sec. IV.

Based on the proposed representation, we can directly generalize the metrics originally developed for random variable relations to analyze complex networks. In this work, we primarily illustrate representative metrics from the perspectives of encoding, decoding, and causal analyses. One can further consider Fisher-Rao metric in information geometry [130, 131] and Wasserstein-2 metric in optimal transport [53, 129–131] in future, both of which can be readily generalized to Gaussian variables.

C. Mathematical relations between our theory and related results

To understand the difference between our work and previous studies [53, 76, 77, 129], we begin with discussing the meaning of the following covariance matrix

$$\Sigma^\heartsuit = L^\dagger + \frac{1}{n}J, \quad (43)$$

which is directly related to the covariance matrix in Refs. [53, 76, 77, 129]. As suggested by Eq. (9), the covariance matrix in Eq. (43) is exactly the inverse of our result $\Sigma = L + \frac{1}{n}J$, i.e., $\Sigma^\heartsuit = \Sigma^{-1}$. If one defines a Gaussian variable $\mathcal{X}_\phi^\heartsuit \sim \mathcal{N}(\mathbf{0}, \Sigma^\heartsuit)$, then its precision matrix Q^\heartsuit equals our proposed covariance matrix

$$Q^\heartsuit := \Sigma^{\heartsuit -1} = \Sigma. \quad (44)$$

Because the partial correlation between $X_\phi^\heartsuit(i)$ and $X_\phi^\heartsuit(j)$, the actual values of $\mathcal{X}_\phi^\heartsuit$ on nodes v_i and v_j , is

fully characterized by the precision matrix [132]

$$\text{corr} \left(X_\phi^\heartsuit(i), X_\phi^\heartsuit(j) \mid \mathcal{X}_\phi^\heartsuit \setminus \{X_\phi^\heartsuit(i), X_\phi^\heartsuit(j)\} \right) := - \frac{Q_{ij}^\heartsuit}{\sqrt{Q_{ii}^\heartsuit Q_{jj}^\heartsuit}} \quad (45)$$

$$= - \frac{\Sigma_{ij}}{\sqrt{\Sigma_{ii} \Sigma_{jj}}}, \quad (46)$$

it is trivial to know that $X_\phi^\heartsuit(i)$ and $X_\phi^\heartsuit(j)$ are expected to have a stronger partial correlation if nodes v_i and v_j are connected by an edge with larger weight (i.e., a larger value of $-\Sigma_{ij}$). Therefore, the Gaussian variable defined by Σ^\heartsuit is more applicable to the cases where edge weights represent node similarity (e.g., see functional brain networks where edges are functional correlations between different cortices [49]). According to Eq. (10), the expected smoothness of mapping ϕ in such a Gaussian variable is

$$\mathbb{E}(\mathcal{S}(\phi)) = \mathbb{E}(\mathcal{X}_\phi)^T L \mathbb{E}(\mathcal{X}_\phi) + \text{tr}(L \Sigma^\heartsuit), \quad (47)$$

$$= \text{tr} \left[L \left(L^\dagger + \frac{1}{n}J \right) \right], \quad (48)$$

$$= \text{tr}(I) - \frac{1}{n} \text{tr}(J) + \text{tr}[L(I - L^\dagger L)], \quad (49)$$

$$= n - 1. \quad (50)$$

Eqs. (49-50) are derived from the fact that $LL^\dagger L = L$ [65] and $LL^\dagger = L^\dagger L = I - \frac{1}{n}J$ [64, 74, 75]. In general, Eqs. (47-50) mean that the expected smoothness of mapping ϕ in a network characterized by $\mathcal{X}_\phi^\heartsuit \sim \mathcal{N}(\mathbf{0}, \Sigma^\heartsuit)$ is independent of the network topology properties conveyed by L . On the contrary, the expected smoothness is fully determined by the network size. We speculate that this property may limit the capacity of $\mathcal{X}_\phi^\heartsuit \sim \mathcal{N}(\mathbf{0}, \Sigma^\heartsuit)$ to describe complex networks with high heterogeneity.

In our results, the Gaussian variable is $\mathcal{X}_\phi \sim \mathcal{N}(\mathbf{0}, L + \frac{1}{n}J)$, where the expected smoothness of mapping ϕ is fully characterized by L via $\mathbb{E}(\mathcal{S}(\phi)) = \text{tr}(LL)$ (see Eq. (14)). The covariance matrix Σ of such a random variable implies that $X_\phi(i)$ and $X_\phi(j)$ are expected to evolve inversely (i.e., stronger negative covariance) if nodes v_i and v_j are connected by an edge with larger weight. In other words, the Gaussian variable defined by Σ is more applicable to the cases where edge weights measure node distance or difference (e.g., see traffic networks where edge weights are distances between locations). Meanwhile, it may have higher potential to characterize heterogeneous networks where node difference matters.

In sum, the proposed covariance matrix $\Sigma = L + \frac{1}{n}J$ and its inverse $\Sigma^\heartsuit = L^\dagger + \frac{1}{n}J$ are applicable to opposite conditions, respectively. In application, one should choose between them according to research demands. Although we primarily use Σ to define encoding, decoding, and causal analyses in our paper, all derived results can

be readily reformulated using Σ^\heartsuit (one only needs to replace L by L^\dagger and replace L^\dagger by L in our formulas). Meanwhile, numerous computational experiments of Σ^\heartsuit have been done by existing studies (e.g., see Ref. [53]). Here we no longer repeat these derivations and experiments. Our released toolbox [59] allows users to choose between Σ and Σ^\heartsuit for a better network characterization. Because real networks inevitably become heterogeneous in certain degrees, we suggest that Σ may also support a promising network representation when edge weights measure node similarity (e.g., see our experiments on real networks in Sec. VII). In the future, one can further conduct more comparisons between these two covariance matrices on empirical data or explore an ideal combination of them.

D. Limitations

As an initial attempt, there certainly remain limitations in our work for further exploration. Here we suggest two limitations whose solutions may significantly advance related fields.

The first limitation arises from the requirements of non-negative edge weights in defining the discrete Schrödinger operator L . There exist numerous real networks whose edge weights can be negative (e.g., in neural populations, excitatory and inhibitory synapses have positive and negative weights, respectively). Although the effects of negative weights on the eigenvalues of L have

drawn increasing attention (e.g., see Refs. [133–135]), an optimal definition of L on networks with negative weights remains rather exclusive. Similarly, the second limitation occurs when one attempts to consider networks with directed edges. While notable progress has been accomplished in defining L on directed networks [136, 137], these achievements can not completely address our problems because an asymmetric version of L do not support the definition of Gaussian variable developed in Sec. III (the covariance matrix Σ must be symmetric). Overall, these two critical limitations should be primarily considered in the future.

ACKNOWLEDGMENTS

Author Y.T. conceptualizes the idea, develops theoretical frameworks, designs computational tools, and writes the manuscript. Authors H.D.H. and G.Z.X contribute equally to literature collection, mathematics proofreading, and manuscript revision. Author Z.Y.Z. contributes to manuscript proofreading and technical support. Author P.S. contributes to idea conceptualization, manuscript writing, and project supervision. This project is supported by the Artificial and General Intelligence Research Program of Guo Qiang Research Institute at Tsinghua University (2020GQG1017) as well as the Tsinghua University Initiative Scientific Research Program.

[1] S. Boccaletti, V. Latora, Y. Moreno, M. Chavez, and D.-U. Hwang, Complex networks: Structure and dynamics, *Physics reports* **424**, 175 (2006).

[2] J. Biamonte, M. Faccin, and M. De Domenico, Complex networks from classical to quantum, *Communications Physics* **2**, 1 (2019).

[3] O. Mülken and A. Blumen, Continuous-time quantum walks: Models for coherent transport on complex networks, *Physics Reports* **502**, 37 (2011).

[4] G. Bianconi, Quantum statistics in complex networks, *Physical Review E* **66**, 056123 (2002).

[5] Y. Roudi and J. Hertz, Mean field theory for nonequilibrium network reconstruction, *Physical review letters* **106**, 048702 (2011).

[6] S. N. Dorogovtsev, A. V. Goltsev, and J. F. Mendes, Critical phenomena in complex networks, *Reviews of Modern Physics* **80**, 1275 (2008).

[7] A. D. Sánchez, J. M. López, and M. A. Rodriguez, Nonequilibrium phase transitions in directed small-world networks, *Physical review letters* **88**, 048701 (2002).

[8] C. Zhou, L. Zemanová, G. Zamora, C. C. Hilgetag, and J. Kurths, Hierarchical organization unveiled by functional connectivity in complex brain networks, *Physical review letters* **97**, 238103 (2006).

[9] E. Bullmore and O. Sporns, Complex brain networks: graph theoretical analysis of structural and functional systems, *Nature reviews neuroscience* **10**, 186 (2009).

[10] C. Li, H. Wang, W. De Haan, C. Stam, and P. Van Mieghem, The correlation of metrics in complex networks with applications in functional brain networks, *Journal of Statistical Mechanics: Theory and Experiment* **2011**, P11018 (2011).

[11] D. S. Bassett and O. Sporns, Network neuroscience, *Nature neuroscience* **20**, 353 (2017).

[12] O. Sporns, G. Tononi, and G. M. Edelman, Theoretical neuroanatomy: relating anatomical and functional connectivity in graphs and cortical connection matrices, *Cerebral cortex* **10**, 127 (2000).

[13] H. Jeong, B. Tombor, R. Albert, Z. N. Oltvai, and A.-L. Barabási, The large-scale organization of metabolic networks, *Nature* **407**, 651 (2000).

[14] A. Wagner and D. A. Fell, The small world inside large metabolic networks, *Proceedings of the Royal Society of London. Series B: Biological Sciences* **268**, 1803 (2001).

[15] R. Tanaka, Scale-rich metabolic networks, *Physical review letters* **94**, 168101 (2005).

[16] H. Jeong, S. P. Mason, A.-L. Barabási, and Z. N. Oltvai, Lethality and centrality in protein networks, *Nature* **411**, 41 (2001).

[17] S.-H. Yook, Z. N. Oltvai, and A.-L. Barabási, Functional and topological characterization of protein interaction networks, *Proteomics* **4**, 928 (2004).

[18] A. Wagner, The yeast protein interaction network evolves rapidly and contains few redundant duplicate genes, *Molecular biology and evolution* **18**, 1283 (2001).

[19] A. Vázquez, R. Pastor-Satorras, and A. Vespignani, Large-scale topological and dynamical properties of the internet, *Physical Review E* **65**, 066130 (2002).

[20] R. Pastor-Satorras and A. Vespignani, *Evolution and structure of the Internet: A statistical physics approach* (Cambridge University Press, 2004).

[21] B. Kahng, Y. Park, and H. Jeong, Robustness of the in-degree exponent for the world-wide web, *Physical Review E* **66**, 046107 (2002).

[22] M. A. De Menezes and A.-L. Barabási, Fluctuations in network dynamics, *Physical review letters* **92**, 028701 (2004).

[23] M. A. de Menezes and A.-L. Barabási, Separating internal and external dynamics of complex systems, *Physical review letters* **93**, 068701 (2004).

[24] M. E. Newman, The structure of scientific collaboration networks, *Proceedings of the national academy of sciences* **98**, 404 (2001).

[25] C. Tsallis and M. P. de Albuquerque, Are citations of scientific papers a case of nonextensivity?, *The European Physical Journal B-Condensed Matter and Complex Systems* **13**, 777 (2000).

[26] F. Menczer, Correlated topologies in citation networks and the web, *The European Physical Journal B* **38**, 211 (2004).

[27] K. Sznajd-Weron and J. Sznajd, Opinion evolution in closed community, *International Journal of Modern Physics C* **11**, 1157 (2000).

[28] A. Pluchino, V. Latora, and A. Rapisarda, Changing opinions in a changing world: A new perspective in sociophysics, *International Journal of Modern Physics C* **16**, 515 (2005).

[29] D. Stauffer and H. Meyer-Ortmanns, Simulation of consensus model of deffuant et al. on a barabasi-albert network, *International Journal of Modern Physics C* **15**, 241 (2004).

[30] S. Soundarajan, T. Eliassi-Rad, and B. Gallagher, A guide to selecting a network similarity method, in *Proceedings of the 2014 Siam international conference on data mining* (SIAM, 2014) pp. 1037–1045.

[31] A. Narayanan, M. Chandramohan, R. Venkatesan, L. Chen, Y. Liu, and S. Jaiswal, graph2vec: Learning distributed representations of graphs, arXiv preprint arXiv:1707.05005 (2017).

[32] N. Attar and S. Aliakbary, Classification of complex networks based on similarity of topological network features, *Chaos: An Interdisciplinary Journal of Nonlinear Science* **27**, 091102 (2017).

[33] D. Conte, P. Foggia, C. Sansone, and M. Vento, Thirty years of graph matching in pattern recognition, *International journal of pattern recognition and artificial intelligence* **18**, 265 (2004).

[34] P. Foggia, G. Percannella, and M. Vento, Graph matching and learning in pattern recognition in the last 10 years, *International Journal of Pattern Recognition and Artificial Intelligence* **28**, 1450001 (2014).

[35] J. Yan, X.-C. Yin, W. Lin, C. Deng, H. Zha, and X. Yang, A short survey of recent advances in graph matching, in *Proceedings of the 2016 ACM on International Conference on Multimedia Retrieval* (2016) pp. 167–174.

[36] X. Gao, B. Xiao, D. Tao, and X. Li, A survey of graph edit distance, *Pattern Analysis and applications* **13**, 113 (2010).

[37] K. Borgwardt, E. Ghisu, F. Llinares-López, L. O’Bray, B. Rieck, et al., Graph kernels: State-of-the-art and future challenges, *Foundations and Trends® in Machine Learning* **13**, 531 (2020).

[38] M. De Santo, P. Foggia, C. Sansone, and M. Vento, A large database of graphs and its use for benchmarking graph isomorphism algorithms, *Pattern Recognition Letters* **24**, 1067 (2003).

[39] T. Cour, P. Srinivasan, and J. Shi, Balanced graph matching, *Advances in neural information processing systems* **19** (2006).

[40] B. Jiang, J. Tang, C. Ding, Y. Gong, and B. Luo, Graph matching via multiplicative update algorithm, *Advances in neural information processing systems* **30** (2017).

[41] O. Enqvist, K. Josephson, and F. Kahl, Optimal correspondences from pairwise constraints, in *2009 IEEE 12th international conference on computer vision* (IEEE, 2009) pp. 1295–1302.

[42] M. Leordeanu, M. Hebert, and R. Sukthankar, An integer projected fixed point method for graph matching and map inference (2009).

[43] M. Zaslavskiy, F. Bach, and J.-P. Vert, A path following algorithm for the graph matching problem, *IEEE Transactions on Pattern Analysis and Machine Intelligence* **31**, 2227 (2008).

[44] N. Shervashidze, S. Vishwanathan, T. Petri, K. Mehlhorn, and K. Borgwardt, Efficient graphlet kernels for large graph comparison, in *Artificial intelligence and statistics* (PMLR, 2009) pp. 488–495.

[45] H. Kashima, K. Tsuda, and A. Inokuchi, Kernels for graphs, in *Kernel methods in computational biology* (MIT Press, 2004) pp. 155–170.

[46] K. M. Borgwardt and H.-P. Kriegel, Shortest-path kernels on graphs, in *Fifth IEEE international conference on data mining (ICDM’05)* (IEEE, 2005) pp. 8–pp.

[47] T. Horváth, T. Gärtner, and S. Wrobel, Cyclic pattern kernels for predictive graph mining, in *Proceedings of the tenth ACM SIGKDD international conference on Knowledge discovery and data mining* (2004) pp. 158–167.

[48] P. Yanardag and S. Vishwanathan, Deep graph kernels, in *Proceedings of the 21th ACM SIGKDD international conference on knowledge discovery and data mining* (2015) pp. 1365–1374.

[49] A. Mheich, F. Wendling, and M. Hassan, Brain network similarity: methods and applications, *Network Neuroscience* **4**, 507 (2020).

[50] C. E. Tomlinson, P. J. Laurienti, R. G. Lyday, and S. L. Simpson, A regression framework for brain network distance metrics, *Network Neuroscience* **6**, 49 (2022).

[51] K. Abbas, E. Amico, D. O. Svaldi, U. Tipnis, D. A. Duong-Tran, M. Liu, M. Rajapandian, J. Harezlak, B. M. Ances, and J. Goñi, Geff: Graph embedding for functional fingerprinting, *NeuroImage* **221**, 117181 (2020).

[52] G. Cimini, T. Squartini, F. Saracco, D. Garlaschelli, A. Gabrielli, and G. Caldarelli, The statistical physics of real-world networks, *Nature Reviews Physics* **1**, 58 (2019).

[53] H. Petric Maretic, M. El Gheche, G. Chierchia, and P. Frossard, Got: an optimal transport framework for

graph comparison, *Advances in Neural Information Processing Systems* **32** (2019).

[54] D. I. Shuman, S. K. Narang, P. Frossard, A. Ortega, and P. Vandergheynst, The emerging field of signal processing on graphs: Extending high-dimensional data analysis to networks and other irregular domains, *IEEE signal processing magazine* **30**, 83 (2013).

[55] A. Sandryhaila and J. M. Moura, Discrete signal processing on graphs, *IEEE transactions on signal processing* **61**, 1644 (2013).

[56] A. Sandryhaila and J. M. Moura, Discrete signal processing on graphs: Frequency analysis, *IEEE Transactions on Signal Processing* **62**, 3042 (2014).

[57] T. M. Cover, *Elements of information theory* (John Wiley & Sons, 1999).

[58] K. Hlaváčková-Schindler, M. Paluš, M. Vejmelka, and J. Bhattacharya, Causality detection based on information-theoretic approaches in time series analysis, *Physics Reports* **441**, 1 (2007).

[59] Y. Tian, H. Hou, G. Xu, Y. Wang, Z. Zhang, and P. Sun, A toolbox for analytic relations between complex networks: encoding, decoding, and causality (2022), open source codes available at <https://github.com/doloMing/Analytic-relations-between-complex-networks-encoding>

[60] T. Biyikoglu, J. Leydold, and P. F. Stadler, *Laplacian eigenvectors of graphs: Perron-Frobenius and Faber-Krahn type theorems* (Springer, 2007).

[61] F. R. Chung and F. C. Graham, *Spectral graph theory*, 92 (American Mathematical Soc., 1997).

[62] R. A. Horn and C. R. Johnson, *Matrix analysis* (Cambridge university press, 2012).

[63] W. Xiao and I. Gutman, Resistance distance and laplacian spectrum, *Theoretical chemistry accounts* **110**, 284 (2003).

[64] P. Chebotarev and E. Shamis, On proximity measures for graph vertices, *arXiv preprint math/0602073* (2006).

[65] J. C. A. Barata and M. S. Hussein, The moore–penrose pseudoinverse: A tutorial review of the theory, *Brazilian Journal of Physics* **42**, 146 (2012).

[66] M. Herbster, M. Pontil, and L. Wainer, Online learning over graphs, in *Proceedings of the 22nd international conference on Machine learning* (2005) pp. 305–312.

[67] G. Wahba, *Spline models for observational data* (SIAM, 1990).

[68] H. Zhang, Y. Xu, and J. Zhang, Reproducing kernel banach spaces for machine learning., *Journal of Machine Learning Research* **10** (2009).

[69] K. Fukumizu, F. R. Bach, and M. I. Jordan, Dimensionality reduction for supervised learning with reproducing kernel hilbert spaces, *Journal of Machine Learning Research* **5**, 73 (2004).

[70] D.-X. Zhou, Capacity of reproducing kernel spaces in learning theory, *IEEE Transactions on Information Theory* **49**, 1743 (2003).

[71] Z. Chen, K. Zhang, L. Chan, and B. Schölkopf, Causal discovery via reproducing kernel hilbert space embeddings, *Neural computation* **26**, 1484 (2014).

[72] N. Brodu and J. P. Crutchfield, Discovering causal structure with reproducing-kernel hilbert space ε -machines, *Chaos: An Interdisciplinary Journal of Non-linear Science* **32**, 023103 (2022).

[73] T. Summers, I. Shames, J. Lygeros, and F. Dörfler, Topology design for optimal network coherence, in *2015 European Control Conference (ECC)* (IEEE, 2015) pp. 575–580.

[74] P. Van Mieghem, K. Devriendt, and H. Cetinay, Pseudoinverse of the laplacian and best spreader node in a network, *Physical Review E* **96**, 032311 (2017).

[75] I. Gutman and W. Xiao, Generalized inverse of the laplacian matrix and some applications, *Bulletin (Académie serbe des sciences et des arts. Classe des sciences mathématiques et naturelles. Sciences mathématiques)* , 15 (2004).

[76] X. Dong, D. Thanou, P. Frossard, and P. Vandergheynst, Learning laplacian matrix in smooth graph signal representations, *IEEE Transactions on Signal Processing* **64**, 6160 (2016).

[77] V. Kalofolias, How to learn a graph from smooth signals, in *Artificial Intelligence and Statistics* (PMLR, 2016) pp. 920–929.

[78] D. J. Bartholomew, M. Knott, and I. Moustaki, *Latent variable models and factor analysis: A unified approach*, Vol. 904 (John Wiley & Sons, 2011).

[79] M. E. Tipping and C. M. Bishop, Probabilistic principal component analysis, *Journal of the Royal Statistical Society: Series B (Statistical Methodology)* **61**, 611 (1999).

[80] S. Roweis, Em algorithms for pca and spca, *Advances in neural information processing systems* **10** (1997).

[81] S. Olver and A. Townsend, Fast inverse transform sampling in one and two dimensions, *arXiv preprint arXiv:1307.1223* (2013).

[82] L. F. Kozachenko and N. N. Leonenko, Sample estimate of the entropy of a random vector, *Problemy Peredachi Informatsii* **23**, 9 (1987).

[83] A. Kraskov, H. Stögbauer, and P. Grassberger, Estimating mutual information, *Physical review E* **69**, 066138 (2004).

[84] K. V. Mardia and R. J. Marshall, Maximum likelihood estimation of models for residual covariance in spatial regression, *Biometrika* **71**, 135 (1984).

[85] L. Malagò and G. Pistone, Information geometry of the gaussian distribution in view of stochastic optimization, in *Proceedings of the 2015 ACM Conference on Foundations of Genetic Algorithms XIII* (2015) pp. 150–162.

[86] A. Casteigts, P. Flocchini, W. Quattrociocchi, and N. Santoro, Time-varying graphs and dynamic networks, *International Journal of Parallel, Emergent and Distributed Systems* **27**, 387 (2012).

[87] M. G. Zimmermann, V. M. Eguíluz, and M. San Miguel, Coevolution of dynamical states and interactions in dynamic networks, *Physical Review E* **69**, 065102 (2004).

[88] S. A. Hill and D. Braha, Dynamic model of time-dependent complex networks, *Physical Review E* **82**, 046105 (2010).

[89] T. Schreiber, Measuring information transfer, *Physical review letters* **85**, 461 (2000).

[90] M. Staniak and K. Lehnertz, Symbolic transfer entropy, *Physical review letters* **100**, 158101 (2008).

[91] Y. Tian, Y. Wang, Z. Zhang, and P. Sun, Fourier-domain transfer entropy spectrum, *Physical Review Research* **3**, L042040 (2021).

[92] A. Shojaie and E. B. Fox, Granger causality: A review and recent advances, *Annual Review of Statistics and Its Application* **9**, 289 (2022).

[93] K. J. Friston, A. M. Bastos, A. Oswal, B. van Wijk, C. Richter, and V. Litvak, Granger causality revisited, *Neuroimage* **101**, 796 (2014).

[94] D. Bueso, M. Piles, and G. Camps-Valls, Explicit granger causality in kernel hilbert spaces, *Physical Review E* **102**, 062201 (2020).

[95] D. Marinazzo, M. Pellicoro, and S. Stramaglia, Kernel granger causality and the analysis of dynamical networks, *Physical review E* **77**, 056215 (2008).

[96] L. Barnett, A. B. Barrett, and A. K. Seth, Granger causality and transfer entropy are equivalent for gaussian variables, *Physical review letters* **103**, 238701 (2009).

[97] R. Davidson, J. G. MacKinnon, *et al.*, *Econometric theory and methods*, Vol. 5 (Oxford University Press New York, 2004).

[98] J. T. Lizier and M. Prokopenko, Differentiating information transfer and causal effect, *The European Physical Journal B* **73**, 605 (2010).

[99] L. Barnett and T. Bossomaier, Transfer entropy as a log-likelihood ratio, *Physical review letters* **109**, 138105 (2012).

[100] N. Ay and D. Polani, Information flows in causal networks, *Advances in complex systems* **11**, 17 (2008).

[101] K. Hlavácková-Schindler, Equivalence of granger causality and transfer entropy: A generalization, *Applied Mathematical Sciences* **5**, 3637 (2011).

[102] J. T. Lizier, M. Prokopenko, and A. Y. Zomaya, Local information transfer as a spatiotemporal filter for complex systems, *Physical Review E* **77**, 026110 (2008).

[103] I. Gutman and B. Zhou, Laplacian energy of a graph, *Linear Algebra and its applications* **414**, 29 (2006).

[104] D. Baruah and A. Bharali, A comparative study of vertex deleted centrality measures, *Ann Pure Appl Math* **14**, 199 (2017).

[105] X.-H. Yang, Q.-P. Zhu, Y.-J. Huang, J. Xiao, L. Wang, and F.-C. Tong, Parameter-free laplacian centrality peaks clustering, *Pattern Recognition Letters* **100**, 167 (2017).

[106] X. Qi, E. Fuller, Q. Wu, Y. Wu, and C.-Q. Zhang, Laplacian centrality: A new centrality measure for weighted networks, *Information Sciences* **194**, 240 (2012).

[107] D. J. Watts and S. H. Strogatz, Collective dynamics of ‘small-world’ networks, *nature* **393**, 440 (1998).

[108] P. Erdős, A. Rényi, *et al.*, On the evolution of random graphs, *Publ. Math. Inst. Hung. Acad. Sci* **5**, 17 (1960).

[109] A.-L. Barabási and R. Albert, Emergence of scaling in random networks, *science* **286**, 509 (1999).

[110] C. Moore and M. E. Newman, Epidemics and percolation in small-world networks, *Physical Review E* **61**, 5678 (2000).

[111] N. Almeira, O. V. Billoni, and J. I. Perotti, Scaling of percolation transitions on erdos-rényi networks under centrality-based attacks, *Physical Review E* **101**, 012306 (2020).

[112] R. Xulvi-Brunet, W. Pietsch, and I. Sokolov, Correlations in scale-free networks: Tomography and percolation, *Physical review E* **68**, 036119 (2003).

[113] G. Csányi and B. Szendrői, Structure of a large social network, *Physical Review E* **69**, 036131 (2004).

[114] N. Zekri and J. P. Clerc, Statistical and dynamical study of disease propagation in a small world network, *Physical Review E* **64**, 056115 (2001).

[115] M. N. Hallquist and F. G. Hillary, Graph theory approaches to functional network organization in brain disorders: A critique for a brave new small-world, *Network neuroscience* **3**, 1 (2018).

[116] K. Zhao, Q. Zheng, T. Che, M. Dyrba, Q. Li, Y. Ding, Y. Zheng, Y. Liu, and S. Li, Regional radiomics similarity networks (r2sns) in the human brain: Reproducibility, small-world properties and a biological basis, *Network Neuroscience* **5**, 783 (2021).

[117] B. Benigni, A. Ghavasieh, A. Corso, V. d’Andrea, and M. De Domenico, Persistence of information flow: A multiscale characterization of human brain, *Network Neuroscience* **5**, 831 (2021).

[118] R. C. Sotero, L. M. Sanchez-Rodriguez, N. Moradi, and M. Dousty, Estimation of global and local complexities of brain networks: A random walks approach, *Network Neuroscience* **4**, 575 (2020).

[119] S. Shirai, S. K. Acharya, S. K. Bose, J. B. Mallinson, E. Galli, M. D. Pike, M. D. Arnold, and S. A. Brown, Long-range temporal correlations in scale-free neuro-morphic networks, *Network Neuroscience* **4**, 432 (2020).

[120] Y. Tian and P. Sun, Percolation may explain efficiency, robustness, and economy of the brain, *Network Neuroscience* , 1 (2022).

[121] C. Martinez-Martinez, J. Mendez-Bermudez, J. M. Rodriguez, and J. M. Sigarreta, Computational and analytical studies of the harmonic index in erdos-rényi models, *MATCH Commun. Math. Comput. Chem* **85**, 395 (2021).

[122] T. Emmerich, A. Bunde, and S. Havlin, Diffusion, annihilation, and chemical reactions in complex networks with spatial constraints, *Physical Review E* **86**, 046103 (2012).

[123] V. Batagelj and A. Mrvar, Pajek datasets (2006).

[124] Y. Du, C. Gao, X. Chen, Y. Hu, R. Sadiq, and Y. Deng, A new closeness centrality measure via effective distance in complex networks, *Chaos: An Interdisciplinary Journal of Nonlinear Science* **25**, 033112 (2015).

[125] M. E. Newman, Scientific collaboration networks. ii. shortest paths, weighted networks, and centrality, *Physical review E* **64**, 016132 (2001).

[126] A. K. Debnath, R. L. Lopez de Compadre, G. Debnath, A. J. Shusterman, and C. Hansch, Structure-activity relationship of mutagenic aromatic and heteroaromatic nitro compounds. correlation with molecular orbital energies and hydrophobicity, *Journal of medicinal chemistry* **34**, 786 (1991).

[127] L. Van der Maaten and G. Hinton, Visualizing data using t-sne., *Journal of machine learning research* **9** (2008).

[128] K. Xu, W. Hu, J. Leskovec, and S. Jegelka, How powerful are graph neural networks?, *arXiv preprint arXiv:1810.00826* (2018).

[129] Y. Dong and W. Sawin, Copt: Coordinated optimal transport on graphs, *Advances in Neural Information Processing Systems* **33**, 19327 (2020).

[130] L. Ning, Smooth interpolation of covariance matrices and brain network estimation, *IEEE transactions on automatic control* **64**, 3184 (2018).

[131] L. Ning, Smooth interpolation of covariance matrices and brain network estimation: Part ii, *IEEE transactions on automatic control* **65**, 1901 (2019).

[132] H. Rue and L. Held, *Gaussian Markov random fields: theory and applications* (Chapman and Hall/CRC,

2005).

[133] S. Ahmadizadeh, I. Shames, S. Martin, and D. Nešić, On eigenvalues of laplacian matrix for a class of directed signed graphs, *Linear Algebra and its Applications* **523**, 281 (2017).

[134] J. C. Bronski, L. DeVille, and T. Ferguson, Graph homology and stability of coupled oscillator networks, *SIAM Journal on Applied Mathematics* **76**, 1126 (2016).

[135] J. Bronski, L. DeVille, and K. P. Koutsaki, The spectral index of signed laplacians and their structural stability, arXiv preprint arXiv:1503.01069 (2015).

[136] F. Bauer, Normalized graph laplacians for directed graphs, *Linear Algebra and its Applications* **436**, 4193 (2012).

[137] R. Agaev and P. Chebotarev, On the spectra of non-symmetric laplacian matrices, *Linear Algebra and its Applications* **399**, 157 (2005).